*Revised Manuscript Unmarked
Click here to view linked References

Dating the Middle Palaeolithic deposits of La Quina Amont (Charente, France) using luminescence methods.

Marine Frouin [1,2*], Christelle Lahaye [2], Hélène Valladas[3], Thomas Higham[1], André Debénath[4†], Anne Delagnes[5], Norbert Mercier [2]

[1] *Research Laboratory for Archaeology and the History of Art, University of Oxford, Dyson Perrins Building, South Parks Road, OX1 3QY Oxford, UK*

[2] *IRAMAT-CRP2A, UMR 5060 CNRS – Université Bordeaux Montaigne – Esplanade des Antilles, 33600 Pessac Cedex, France*

[3] *LSCE/IPSL - UMR CEA-CNRS-UVSQ, Domaine du CNRS, Avenue de la Terrasse, 91190 Gif-sur-Yvette, France*

[4] *HNHP, UMR 7194, Université de Perpignan Via Domitia, 66860 Perpignan Cedex 9, France*

[†] *Deceased 3 June 2016*

[5] *PACEA, UMR 5199, Université de Bordeaux, Allée Geoffroy St Hilaire (B8), CS50023, 33625 Pessac Cedex, France*

[*]corresponding author: marine.frouin@rlaha.ox.ac.uk

Abstract

The La Quina Amont site, located in the Charente region, is one of the most important sites in southwestern France for studying major changes in human behaviours from the Middle Palaeolithic (MP) to the Early Upper Palaeolithic (EUP). Extensively excavated over the past 50 years, numerous dating studies have been focused on the Upper Palaeolithic deposits using radiocarbon on bone collagen and thermoluminescence (TL) on heated flints; however, the Mousterian levels remain undated due to the scarcity of suitable materials. Our investigations aimed to provide for the first time a chronological framework for the site using luminescence dating methods on different minerals contained in the sediments. Coarse grains of quartz were dated using optically stimulated luminescence (OSL) technique, and polymineral fine grains were dated using both infrared (IRSL) and post-infrared (pIR-IRSL) stimulated luminescence signals. OSL, IRSL and pIR-IRSL results were combined with available TL and radiocarbon data sets to propose a chronology for the site. The agreement between these methods provides key insights into the sedimentological processes involved in the site formation and into the chronology of the human occupations. In particular, it shows that the sequence spans almost ~20,000 years (20 ka). Moreover, the new chronological framework suggests that the makers of the Quina lithic technocomplex (LTC), who were reindeer hunters, inhabited the site from the end of marine isotope stage (MIS) 4 to the beginning of MIS 3. We also show that Levallois and Discoidal industries occurred successively under temperate palaeoclimatic conditions, during MIS 3 but not after ~40 ka. Finally, we compare the Quina LTC dataset with other sites in southern France in order to shed light upon the variability in Mousterian industries of this region.

Keywords: Luminescence dating; Middle Palaeolithic; Quina; lithic technocomplex.

1. Introduction

The site of La Quina located in the Charente region in southwest France (Fig. 1) has been known for a century for its rich record of Palaeolithic artefacts, which constitute an important source of information for the study of Pleistocene human settlements in the region (Henri-Martin, 1966; Debénath and Jelinek, 1998; Bierwirth, 1996; Jelinek, 2013). Lithic and faunal materials contained in the deposits have contributed significantly to our knowledge of the lifeways of the human groups who inhabited the site over many millennia. The site also gives its name to a large scraper industry found in the southern part of the site, which was described for the first time by Bordes (1953), and then recognized elsewhere. This Quina Mousterian industry – or Quina lithic technocomplex (LTC) – occurs in association with cold period fauna at the site, and is, consequently, considered to have taken place during a cold climate phase, marine isotope stage (MIS) 4, about 71 - 60 ka; the tools being made by successive hunter-gatherer groups (e.g. Delagnes and Rendu, 2011). Moreover, the exceptional preservation of human remains, including a complete Neanderthal adult skeleton, has enabled paleoanthropologists to document aspects of the development of Neanderthal morphology (Martin, 1923; Henri-Martin, 1966; Stefan and Trinkaus, 1998; Verna et al., 2010). The La Quina Amont site plays an important role in discussions about the variability of Mousterian technologies across time and space and offers an excellent context for further investigation into some of the questions about Neanderthal subsistence strategies and mobility pattern. A reliable chronology is key if we are to understand Middle Palaeolithic lithic variability throughout this time period and its relationship to change in palaeoclimate and palaeoenvironment.

Radiocarbon dating has been applied since the 1960s, when excavations were first carried out in the northern part of the complex (Henri-Martin, 1966; Debénath and Jelinek, 1998; Jelinek, 2013). In the last decade, developments in sample pre-treatment chemistry for AMS dating have shown that most previously available age determinations are erroneously young, due to small amounts of modern ^{14}C contamination (Higham, 2011). Recently, two radiocarbon dating campaigns have been conducted (Park, 2007; Higham et al., 2014) and the dates indicated that the northern part of the deposits (Layers 8 to 2) starts beyond the radiocarbon limit ~45 ka cal BP (Before Present) and ends at ~40 ka cal BP (Table 1). Other dating methods have also been applied. In 1999, for example, four burned flints were selected during excavations for thermoluminescence (TL) dating (Mercier and Valladas, 1999). Layer 6a yielded two statistically indistinguishable TL ages with an average of

43.0 ± 3.6 ka (sample Q3 and Q1). Two flints have been dated from Layer 8, giving ages ranging from 45.5 ± 4.2 ka (Q14) to 53.0 ± 5.0 ka (Q15). The authors considered the date of the Q15 sample as less reliable because of its relatively lower internal dose rate compared to other samples, implying a greater dependence on environmental dose variations over time. On the basis of these results, summarized in Table 1, and following the faunal association proposed by Chase et al. (1994) and Debénath and Jelinek (1998), the northern part of the La Quina sequence has been attributed to MIS 3. However, the second area, which is located in the southern part of the site (Fig. 2), is believed to date well beyond the ^{14}C age limit (~50 ka). Therefore, the complete sequence stratigraphic of La Quina site and its eponym lithic technocomplex remain undated.

Over the last two decades, the optically stimulated luminescence (OSL) dating method has been increasingly used to date Late Pleistocene archaeological sites in cave, rock shelter or open-air contexts (e.g. Liritzis et al., 2013). By measuring the time elapsed since minerals were last exposed to daylight, it allows the direct dating of sediments associated with archaeological remains and periods of human occupation at an individual site. In this paper, we compare luminescence dates obtained from coarse grains of quartz with those from fine grains of feldspar, both extracted from La Quina Amont deposits. Luminescence results are then combined with available TL and radiocarbon data sets to establish a new chronological framework and, therefore, for the first time, enable the examination of the timing of human activities and occupations at La Quina. The chronology of the lithic production systems identified at the site is discussed in regard to other late Middle Palaeolithic sites in southwest France.

HERE FIG. 1 & 2

2. La Quina site

2.1 Location and brief excavation history

La Quina extends more than 300 metres along the foot of a limestone cliff flanking the Voultron River (Fig. 3). There are three separate loci of interest. Locus 3 is a complex of small caves located on the top of the cliff, which was discovered and excavated in 1872 by G. Chauvet. Unfortunately, little information is available about these excavations. During this period, Chauvet distinguished two other loci, later designated by L. Henri-Martin in the 1900s as Station Amont (“upstream”; locus 1 in Fig. 3) and Station Aval (“downstream”; locus 2 in Fig. 3). Both areas were extensively excavated in the decade following the site’s

discovery, successively by M. Vergnaud, R.-A. Fournier, M. Condamy and, principally, G. Chauvet and M. Ramonet, and finally, by L. Henri-Martin and his daughter, G. Henri-Martin. The Martins excavated a series of trenches starting near the road, which went progressively deeper in the direction of the cliff: these trenches are named A to M at Station Amont and X-Y-Z at Station Aval. In the trenches at Station Amont, several metres of archaeological sequences containing well-defined levels of Mousterian occupations were observed. In Station Aval, levels of Chatelperronian and Aurignacian occupations were also identified.

Between 1985 and 1994, A. Debénath and A. Jelinek led an international multidisciplinary team in renewed excavations at the site. The main objectives were to improve the chronology of the deposits and obtain information on the palaeoenvironmental background to the occupation in the upper Pleistocene. Our study focuses on Station Amont and, more particularly, on trenches C-D (Fig. 2), the most complete sections of the sequence.

HERE FIG. 3

2.2 Stratigraphy of Station Amont

Lithostratigraphy and sedimentary dynamics

The stratigraphic sequence originally defined by A. David in 1987 has not been significantly amended since its publication in 1998 (Debénath and Jelinek, 1998). A detailed study of the sediments was initially undertaken by T.D. Young but has not been resumed and remains unpublished. Small portions of his studies have been incorporated in Jelinek (2013).

Station Amont is divided into northern and southern deposits. Twenty-five layers have been distinguished throughout the deposit. Table 1 provides a description of the stratigraphic units based on the excavations of A. Debénath and A. Jelinek. We report here the description of the major depositional units and their sedimentary dynamics (Jelinek, 2013), from the base to the top:

At the base of the southern deposit, above a sterile deposit, Layers O to P are predominantly quartz sands intercalated with lenses of clayey silt, resulting from occasional flooding of the Voultron River, at the time when its level was 2 m higher than at present. Limestone blocks of different sizes, weathered from the cliffs above, are present throughout these layers. Layer N is composed of greenish grey sandy clay of fluvial origin. The predominance of clay in Layer M and L may reflect accumulation during seasonal inundation with periodic exposure to the atmosphere but the clay could also has been derived from weathered sediments on the cliff ledges and plateau above. The following colluvial Layers K

and J have been interpreted as resulting from a frost weathering of the cliffs and erosion of sediments above the site. Then, the deposit is formed by a steeply sloped accumulation, formed by a succession of primarily limestone blocks layers from the relatively coarser sediments of Layer G3 up to the finer sediments of Layer G1. The brecciated consolidation of sediments in these layers suggests periods of percolation of water.

In the northern part of the deposit, the position of Layer 8 shows a sudden and drastic change in depositional regime in this portion of Station Amont in front of the overhanging lowest cliff scarp. This layer is constituted predominantly by anthropogenic content mixed with relatively small limestone blocks clasts and fine sediment. The yellowish Layer 7 consists almost entirely of limestone blocks clasts of moderate to small size, reflecting a significant period of weathering of the cliff by frost. Layer 6 is divided into four sub-layers: Layer 6d is distinctly lighter in colour than the overlying Bed 6c, which appears to have a higher quantity of limestone blocks but is distinctly darker in colour (due to the presence of organic carbon) than Layer 6a or 6b. Layer 5 has been interpreted as resulting from a temporary drainage channel down the cliffs and Layer 4, containing large pieces of animal bone and scattered flint artefact in a clayey matrix, may represent a shift toward more temperate conditions than previously. Meanwhile, the large quantity of coarse material provides evidence of considerable rockfall. Finally, Layers 3 and 2 complete the last part of the sequence in the niche under the overhanging cliff. They contain some evidence of human activity, with lithic artefacts and abundant large pieces of animal bone in a matrix of limestone clasts.

Faunal remains and palaeoenvironment

In Station Amont, three taxa dominate the faunal assemblages (Table 1): reindeer (*Rangifer tarandus*), horse (*Equus caballus*) and large bovids (mainly bison, *Bison priscus*). In the southern part of the sequence (Layers M-N), reindeer is dominant (percentage of NISP [Number of Individual Specimens]: 90% of identified faunal remains) with decreasing proportions of bison and horse to reindeer from Layer L (NISP: 30%) to F (10%). The presence of reindeer throughout the sequence indicates a very cold climate and vegetation that is characteristic of the marginal boreal taiga. In the northern sequence, reindeer is still present but in various amounts throughout the sequence. Reindeer dominates Layers 8 and 7 at the base of the sequence. Layer 8 contains the maximum number of reindeer (NISP: 90%) along with the presence of red fox (*Vulpes vulpes,* NISP: 2), which may indicate the coldest environment of the sequence. Layer 6 is dominated by large bovids (NISP: 60%),

reindeer (20%) and horses (10%). Such an assemblage usually implies nearby open terrain and grassland. The presence of *Cervus*, in decreasing frequencies from 6d to 6a, in conjunction with the presence of wild boar (*Sus scrofa,* NISP: 1) in Layer 6d, may indicate that this layer was the most temperate of the sequence. The dominant presence of reindeer again in Layer 5 may reflect a return to colder conditions. Finally, Layers 4 and 2 are dominated by horse, with bovid and reindeer in lesser proportions.

Zooarchaeological analyses have demonstrated that the concentration of faunal remains was the result of human activity (Chase et al., 1994). However, other agents, such as carnivore activity, action of stream flow and taphonomic agents, were responsible for the final configuration of the archaeological assemblages, with each one in turn imposing a different patterning on the material. Given the information we have, it is not possible to quantify the effects of each agent. Therefore, it is still difficult to know whether the site was mainly a kill site or a consumption site. Moreover, the lack of patterning relative to the treatment of reindeer carcasses throughout the sequence is likely to indicate mixing of activities.

Lithic assemblages

The excavations between 1985 and 1992 allow the examination of the sedimentary deposits and the archaeological material at Station Amont (trenches C-D). A brief description of the assemblages, from the bottom to the top of the sequence, is provided (Jelinek, 2013):

At the base of the southern sequence, Layers P and O yielded the earliest cultural evidence, but only a few, widely scattered flint and quartz artifacts were recovered, probably deposited at different times. In contrast to the underlying sand, lithic artefacts were abundant in Layer N. The heavy concentration of remains in this layer might indicate a longer period of deposition, which attests to the presence of human activity. Layer N shows the highest presence of scrapers (91.3%), mainly transverse scrapers made on short flakes, with a high proportion of lateral scrapers, with scalariform retouch and convex edges. The other tools are: a single piece classified as an elongated Mousterian point, one denticulate and two notched pieces. The lithic assemblages from Layers N to G are attributed to the Quina lithic technocomplex. The main difference between each layer is the frequencies of lateral or transverse scrapers. Through these layers, the presence of scraper retouch flakes attests to frequent edge resharpening, probably as part of intensive butchering activities, as herbivore bones are also very abundant. Layer M is dominated by lateral and transverse scrapers in equal frequency. It contains only few poorly retouched pieces. The proportion of

notches and denticulates is relatively high among the retouched pieces (25%). In Layer L, the scrapers represent 84% of the tools. The lateral scrapers dominate the assemblage and the transverse scrapers are present in fewer numbers. The scalariform retouch and convex edges are important and denticulates are present. Layer G is divided into three sub-layers. Denticulates and notches are present in Layers G1 and G2, but absent in G3. Layer G3 is characterised by a high number of scrapers (more than 88% of the assemblage).

In the northern deposits, the lithic assemblage is dominated by denticulates and notched pieces in Layers 8, 7 and 2, and is, consequently, classified as a Denticulate Mousterian industry using alternately a Levallois or Discoid technology. The Discoidal method increases at the top of the deposit. In the upper sequence, Layer 6d is classified as a Mousterian of Acheulean Tradition assemblage (Debénath and Jelinek, 1998), based on the presence of a few bifaces, fragments of bifaces and shaping flakes.

Human remains

Over the different excavations at Station Amont, a total of 53 human remains have been discovered. All of them show characteristics which allow us to link them with the Neanderthal lineage (Martin, 1923; Henri-Martin, 1966; Verna et al., 2010). Among the remains is a complete skeleton found in 1911 at the base of the stratigraphy, in trench B, near the base of the cliff. It was interpreted by H. Martin as being the result of an accidental drowning and/or a rapid burial of a body thrown into the river. The fact that this skeleton has been entirely preserved has been seen as an indication of a deliberate burial (Verna, 2007). From trench B/C, the fragment of a child's frontal bone and a portion of an adult calotte have also been found in the lower beds (associated with the Quina industry), as well as several teeth.

3. Material and methods

Several studies have shown the advantages of using a combined approach in dating a variety of materials, using different luminescence methods to date Palaeolithic sites (e.g. Mercier et al., 2007; Guérin et al., 2012a, 2015; Richter et al., 2013; Frouin et al., 2014). At La Quina, burned flints had already been dated from parts of the site with the TL method, so we decided to focus on the dating of sediment grains to establish a chronological framework for the entire sequence.

3.1 Sampling

In January 2012, a series of 12 samples was collected along the entire sequence. The sediment compaction and the abundance of limestone blocks did not allow the insertion of opaque tubes in the sections, therefore the sequence was thoroughly cleaned and the sampling undertaken by scratching the sediment with a trowel, under an artificial shelter (with opaque plastic tarp) and using controlled red lighting. The entire sequence was thus able to be protected from leaching, weathering and from direct sunlight exposure. During sampling, a sub-sample of sediment was collected in transparent bags for measurement of moisture content and radioelement contents. Sediments preserved from light were collected in opaque plastic bags. Their location on the stratigraphic sections is shown in Figure 4.

HERE FIG.4

3.2 Preparation and analytical facilities

In the laboratory, under controlled light, each sediment sample was prepared in the conventional manner to extract suitable grains for luminescence dating (Wintle, 1997). In order to identify the most widely represented granulometric fraction, each sample was analysed with a laser diffraction granulometer. Granulometric profiles for all samples show a bimodal distribution (Fig. 5). The quantities of material available were small, so we decided to select the 20 – 41 µm polymineral fraction, rich in potassium feldspars, for IRSL measurements, and in parallel, purified the 160 – 250 µm fraction in order to isolate quartz grains. To isolate these size fractions, the samples were wet-sieved after an ultrasonic bath (Branson, type 5250) with a sodium hexametaphosphate solution. Then, the selected fractions were treated with hydrochloric acid (10 % HCl) and then with hydrogen peroxide (30% H_2O_2) for 24 h to remove carbonates and organic matter, respectively. For the coarse grain fraction, a density separation (between 2.70 $g.cm^{-3}$ and 2.62 $g.cm^{-3}$) was employed in order to isolate a rich quartz fraction, which was purified with a mixture of hexafluorosilicic (30% H_2SiF_6) and nitric (HNO_3) acids for a week and then rinsed with HCl. This chemical treatment dissolved of feldspar and feldspathoid grains. After rinsing, drying and sieving, the polymineral fine fraction was mounted on stainless steel cups and the quartz-rich fraction was fixed onto disks using silicone spray (aliquot diameter 4 mm), for the luminescence experiments designed to determine the equivalent dose of each sample.

Luminescence measurements were performed with an automated Risø TL/OSL DA-15 reader (Bøtter-Jensen et al., 2003) equipped with a $^{90}Sr/^{90}Y$ source that delivered a dose rate of 0.123 ± 0.002 $Gy.s^{-1}$ to the material deposited in the cups and 0.152 ± 0.003 $Gy.s^{-1}$ to quartz grains fixed to the disks. To stimulate the feldspar grains contained in the polymineral fine fraction, we used infrared light emitting diodes (Vishay TSFF5210), emitting at 870 nm (Bøtter-Jensen et al., 2003). The luminescence signals were detected with an EMI 9235 QA photomultiplier tube (PMT) through a combination of optical filters (Schott BG39 [2 mm] colour glass filter and Corning type 7-59 [4 mm, passband 320 nm to 430 nm; 50% transmission]). The recorded signal is assumed to be dominated by K-rich feldspars (Huot and Lamothe, 2012). The quartz OSL signal was stimulated with the emission from blue LEDs (NICHIA type NSPB-500AS) emitting at 470 ± 30 nm associated with a long pass filter (Schott GG420 [3mm]). The resulting signal was detected through an optical filter (Hoya U-340 [7.5 mm]) used in front of the PMT. All the measurements were performed under nitrogen atmosphere.

HERE Fig 5

3.3 Dosimetry

The doses of radiation to which the grains have been exposed during burial originate from the decay of natural radioelements (mainly from U- and Th-series, and from K), which emit ionizing particles: alpha and beta particles and gamma rays. In addition, the minerals are also continuously irradiated by cosmic rays. The annual dose takes into account these contributions, and can be divided into two parts: the radiation sources coming from the material itself (internal contribution) and from its environment (external contribution).

In the case of the coarse quartz grains, the internal dose has been ignored since this mineral is assumed to contain very low amounts of radioelements (~1 p.p.b, i.e. 0.001 µg/g) in comparison to the usual contents of sediments (typically 0.1 to 1 µg/g). For K-feldspars, an internal dose has been calculated assuming a 10 ± 2 % potassium content and a 400 ± 100 ppm rubidium content (Huntley and Hancock, 2001; Readhead, 2002). The conversion factors were taken from Guérin et al. (2011) and the grain size attenuation factors from Guérin et al. (2012) for quartz and feldspar. For the alpha dose rate calculation, an alpha efficiency of 0.08 ± 0.02 was assumed (Rees-Jones, 1995) since the polymineral fine grains were not etched. The relative sensitivity of quartz to alpha compared to beta rays was assumed to be 5 $\mu Gy/10^3$ $alpha/cm^2$, following Tribolo et al. (2001).

The external beta dose rate contribution for quartz and feldspar was calculated from the K, U, Th contents of each sample. A portion of dry sediment was homogenised by crushing in an agate mortar, then compacted and sealed in plastic boxes containing ~8 g of sediment. After at least three weeks of storage, the boxes were measured with a high resolution, low background gamma spectrometer (Guibert and Schvoerer, 1991). For each sample, the amount of K, U and Th content was deduced from the activity of the radionuclide present (^{238}U, ^{235}U, ^{232}Th and daughters, and ^{40}K). In order to evaluate the state of disequilibrium of the U-series chain, we need to compare the effective U contents of the top of the decay chain (^{234}Th, ^{234m}Pa, and ^{235}U) with the bottom (^{214}Pb and ^{214}Bi). In the case of a closed system, the U-series is in secular equilibrium, i.e. both effective U contents are the same (Guibert and Schvoerer, 1991). In our samples, this ratio is within 5% of the unity, which indicates that no significant disequilibrium affects the sequence (Supplementary Online Material [SOM] Fig S1). The beta dose-rate was then calculated based on the bottom of the U-chain value, which contributes to ~90% of the total dose (Aitken, 1998).

The effect of moisture on beta dose rates was calculated following Nathan and Mauz (2008). However, the moisture content measured immediately after sampling is different from the moisture content of the sediment during the time it was buried. It is thus necessary to determine what the moisture content may have been during this period. For La Quina samples, the measurement of water saturation content yielded maximum values of ~30 %, on average. We took 0.5 ± 0.2 as a representative value for the fraction of saturation, leading to a past moisture content of 15 ± 5 % (at 1 σ). Thus, the range of 5-25 % (at 2 σ) covers all reasonable possible water content scenarios during burial time. For Layers M to R, the presence of green clay and hydrous iron and manganese oxides on the flints and bones (Jelinek, 2013) suggests repetitive overflows of the river in the past. For these Layers, a moisture content of 30 ± 5 % (1σ) was considered.

Cosmic and gamma dose rates were determined from the measurement of the luminescence signal recorded by dosimeters buried in the sequence, in close proximity to the location of the sediment samples (Fig. 4). A dosimeter consists of three pellets of carbon-doped aluminium oxide (Al_2O_3:C, diameter: 5 mm, thickness: 1 mm) placed at the extremity of a metal tube of ~30 cm in length. Before burial, the pellets were heated at 350°C to reset any remaining luminescence signal. The OSL signal measured in the laboratory was compared to those induced by an artificial beta source which was calibrated using a reference block (Mercier et al., 1994). The measured dose corresponds to a period of burial of 166 days. Each pellet was measured using a Daybreak 2200 OSL reader system

(Bortolot, 2000) combining green light stimulation (Nichia NSPG310) and 7.5 mm Hoya U-340 filters for detection. The gamma dose rates obtained from these dosimeters are considered to be more representative of the radioactive environment surrounding the dated materials because they characterize a bigger volume than the sediment samples analysed with the high-resolution gamma-spectrometry (Guerin et Mercier, 2011).

4. Results

4.1 Annual dose

The radioelement contents determined from the gamma spectrometric measurements and the related dose rates derived according to Guérin et al. (2011) are given in Table 2. The feldspar grains have been exposed to dose rates ranging from 0.97 ± 0.04 $Gy.ka^{-1}$ (BDX 15259) to 2.41 ± 0.08 $Gy.ka^{-1}$ (BDX 15273). The quartz grain dose rates are less scattered and range from 0.58 ± 0.03 $Gy.ka^{-1}$ (BDX 15263) to 1.17 ± 0.02 $Gy.ka^{-1}$ (BDX 15271).

HERE TABLE 2

4.2 IRSL and post-IR IRSL protocols on polymineral fine grain fraction

For luminescence dating purposes, K-feldspars are known to provide a suitable alternative to quartz. However, routine use of feldspars is hampered by the anomalous fading effect (Wintle, 1973; Spooner, 1994) which is sample dependent (Lamothe et al., 2012; Trauerstein et al., 2012) and leads to an age underestimation if it is not corrected for or circumvented (Aitken, 1985). If the IRSL signal (measured at 50 °C, hereafter IR_{50}) usually fades by 3 - 5 % per decade of time (Auclair et al., 2003), the elevated temperature post IR-IRSL signal (pIR-IRSL) allows us to overcome this problem or, at least partly, reduces its effect. In particular, the pIR-IRSL signal measured at 225 °C (hereafter pIR-IR_{225}), following a prior IRSL stimulation at 50 °C (SOM Table S1), has a lower fading rate, and a low residual dose. Buylaert et al. (2012) reported a residual dose of 4.1 ± 1.1 Gy for well-bleached polymineral fine grain samples. Comparable residual doses of ~2 Gy (Buylaert et al., 2009) on coarse grains and ~5 Gy (Chen et al., 2013) have also been reported for well-bleached samples from various origins. At La Quina, an unbleachable residual dose of ~3 Gy was measured after a 2 h stimulation with a SOL500 solar simulator. We decided to calculate the pIR-IR_{225} ages corrected and not corrected for the residual dose before fading correction.

In order to confirm the reliability of the SAR protocols, beta-dose recovery tests were carried out on three aliquots of one sample (BDX 15263). After exposure to a solar

simulator (SOL500) for 2 h, a given dose of 80 Gy was delivered to the aliquots and the dose was subsequently measured using the IR_{50} and pIR-IR_{225} signal, corrected ($_{rc}$) and uncorrected for the residual. The measured to given dose ratios (dose recovery ratios; SOM Fig S2) are consistent with unity with, on average, 0.99 ± 0.06 (IR_{50}), 0.99± 0.06 (pIR-IR_{225}) and 0.98 ± 0.06 (pIR-IR_{225rc}), thus indicating the suitability of the applied SAR protocols with or without the residual correction. The equivalent doses were determined using the IR_{50} signal for 12 samples and the pIR-IR_{225} signal for 10 samples (the quantity of datable material was not sufficient to apply both protocols to each sample). The luminescence signals were obtained by integrating the first 5 s and 2.5 s of the IR_{50} and pIR-IRSL signals, respectively, and the background, determined on the last 10 s in both cases, was subtracted. The standard SAR protocols have been applied using four regenerative doses and a zero dose cycle. The growth curve was fitted with a single saturating exponential function using the Analyst software (Duller, 2007). The criteria for validating the application of the SAR protocol relies on the recycling ratio (1.00 ± 0.05 for our samples) and the recuperation ratio (< 5 %), which have been met for all of our samples. In practice, for both protocols, the natural signal is interpolated onto the growth curve to obtain the D_e, which is situated well below the saturated luminescence level (Fig. 6 a-b). The overdispersion (OD) values for both signals, determined by the Central Age Model (CAM; Galbraith et al., 1999), are between 0 and 9 ± 3%. The weighted mean IR_{50} and pIR-IR_{225} equivalent doses at one sigma (Table 3) were calculated for each sample as the average dose of 6 to 12 aliquots. The distributions of equivalent doses are reported in SOM Figs. S5 and S6. For example, the D_e distributions for sample BDX 15261 are given in Fig 6d and 6e. The uncertainties on an individual D_e have been determined using classical rules of error combination using the Analyst software (Duller, 2007). The standard deviation takes into account the contributions from counting statistics and the curve fitting error.

Correction for anomalous fading was necessary to avoid any underestimation of the ages. The fading rate was measured for each sample on bleached aliquots by comparing the IRSL signal immediately after an irradiation (t=0) to the signal obtained after a defined interval of time. The decrease of the signal with time generates a straight line on a logarithmic scale, the slope of which corresponds to the fading rate (Aitken, 1985). These analyses were performed on the aliquots previously measured to obtain the D_e and after a 2 h bleach with the solar simulator in order to cleanout any residual signal (Auclair et al., 2003). A dose of ~50 Gy was given and repeated L_x/T_x cycles were carried out with different delay times inserted after the preheating of the regenerative dose (Auclair et al., 2003).

Time delays varied from 0.09 h to 21 h and from 0.15 h to 22 h, for the IR_{50} and pIR-IR_{225} measurements, respectively. Fading rates of the IR_{50} signal measured on all samples range between 1.79 ± 0.46%/decade (BDX 15265) and 2.70 ± 0.26%/decade (BDX 15263). The fading rate of the pIR-IR_{225} signal was measured on eight samples. For four samples (BDX 15259, -61, -71 and -72), the fading rates were around ~1.15%/decade, whereas for the four others (BDX 15263, -66, -67, -70), fading rates were consistent with zero, therefore considered as negligible. For samples BDX 15265 and 15269, fading experiments have not been carried out and their rates were assumed to be close to those obtained for feldspars contained in the overlying and underlying layers because the nature and the origin of the sediment, in this part of the site, are considered to be identical (Jelinek, 2013). Therefore, no fading correction has been applied for these two samples. In other cases, a fading correction has been applied using the Eq. (A5) of Huntley and Lamothe (2001).

HERE Fig. 6

TABLE 3

4.3 OSL on quartz

The OSL signal from the La Quina quartz is dominated by the fast component (identified as C1 in SOM Fig S3). The net intensity used for building the growth curve was derived from the OSL signal integrated over the first 0.8 s of stimulation minus the last 8 s. The effect of IR stimulation at 125 °C during 100 s has been tested on each sample and showed no significant signal (IR depletion ratio = 1.00 ± 0.15). This indicates that feldspars do not significantly contaminate the quartz fraction. A standard SAR dose protocol has been applied using four regenerative doses, and a test dose for normalisation. A regeneration dose equal to the first one was repeated during the last SAR cycle in order to obtain a recycling ratio, which gives information on the sensitivity change correction efficiency. All recycling ratios were within 10% of unity for all aliquots. Recuperation was checked using a zero dose cycle after measurement of the largest regeneration dose and showed no significant signal transfer (always less than 5 % of the normalized natural signal).

Dose recovery tests were carried out on each sample, using different temperature conditions. The aliquots have been bleached under a Hönle SOL500 solar simulator for 1 h and a regenerative dose of 55 Gy was given. The preheat tests were conducted between 220 °C and 280 °C (with steps of 20 °C) for 10 s prior to luminescence measurements performed at 125 °C for 40 s. After irradiation with the test dose (which represented ~ 30 %

of the first regenerative dose), a short heat (cutheat) was applied at lower temperature, which has been fixed at 160 °C. Between two successive cycles, a stimulation at 280 °C held for 40 s was applied. For some samples, a cutheat to 160 °C seems to underestimate the given dose; so we performed a second series of recovery tests, increasing the cutheat temperature at 180 °C. For the sample that failed the first recovery test, the average measured/given dose recovery ratio is within 10% of unity when increasing the cutheat temperature. Fig. 7 shows preheat plateaus obtained for samples BDX 15263 and BDX 15267, respectively, during recovery tests. The suitable preheat and cutheat temperature conditions have been selected for each sample following these recovery tests. These parameters are reported in Table 3.

The quartz from La Quina met all the laboratory-based criteria for the applicability of a SAR protocol. The equivalent doses and their uncertainties were estimated by interpolating the normalized natural OSL signal onto the normalized regenerated growth curve (Fig. 6c), fitted with an exponential function using Analyst software (Duller, 2007). For all samples the natural signal is situated well below the saturated luminescence level (Fig. 6.c and SOM Fig S4). Between 16 and 24 aliquots were measured for each sample in order to get an equivalent dose distribution. For example, the D_e distributions for sample BDX 15261 are given in Fig 6f and for all samples in SOM Fig. S7. The OD values determined by the CAM are between 8 ± 2% and 20 ± 4%. Other studies have also reported up to 20% overdispersion among D_e estimates for single aliquots and individual grains of quartz that are known to have been well bleached in the past (Roberts et al., 2000; Olley et al., 2004; Thomsen et al., 2007; Galbraith and Roberts, 2012). We therefore considered that the quartz samples were well bleached and calculated the weighted mean D_e value for each of the samples using the CAM with a precision of 1 sigma (Table 3).

HERE Fig 6

HERE Fig 7

4.4 Age results and discussion

The polymineral and quartz ages reported in Table 3 and displayed in Fig. 8 appear to be in overall good agreement with the stratigraphic sequence. As expected, the residual uncorrected pIR-IR_{225} ages overestimate the pIR-IR_{225} corrected ages but the difference is limited to between 2 and 5%. Meanwhile, the pIR-IR_{225} corrected ages appear to be in better agreement with other results, indicating that the subtraction of the residual dose has to be considered for these samples.

In the northern sequence, the ages range from 44.9 ± 3.2 ka (OSL - BDX 15259) for Layer 6 to 55.5 ± 2.2 ka (IR_{50} - BDX 15262) for Layer 8, whereas in the southern sequence, the ages are all consistent with an average age of 56.5 ± 4.2 ka (OSL and IR_{50}) considering their uncertainties and excluding the OSL age of BDX 15271. When looking in detail at these results, it appears that the age of sample BDX 15267 (Layer G2) is underestimated. The quartz OSL age (43.1 ± 2.6 ka) is consistent with the IR_{50} age (46.7 ± 3.0 ka) at 1 sigma and with the pIR-IR_{225} age (53.2 ± 3.8 ka) at 2 sigma. The reason for this underestimation is not clear. A discrepancy between the quartz and feldspar results could have two major origins: i) insufficient bleaching (mainly of feldspars) or ii) an inaccurate determination of the total dose rate. If the sample was significantly affected by incomplete bleaching, it would be likely that large multi-grain aliquot measurements would result in an overestimate of deposition age, because each aliquot contains both well-bleached and poorly bleached grains. But in the present case, both the coarse quartz and the K-feldspar ages are underestimated in comparison with samples located above and below. Moreover, because IR_{50} and pIR-IR_{225} ages are consistent within one sigma, it is likely that the feldspar grains were sufficiently bleached at the burial time. As a consequence, it seems that our first hypothesis must be ruled out, whereas our second hypothesis makes more sense. The present dose rate, especially its beta component, might not be representative of the dose rates received by the grains during their burial. Furthermore, it is interesting to note that the total dose rate in Layer G2 is much higher than the values measured for other sediment samples (about twice as high), linked to high values of both the gamma and the external beta dose. The reason for such high values is not well understood and, in terms of dating, it seems safer to consider the age of sample BDX 15267 as merely indicative, in comparison to the other results.

It is also informative to compare quartz and feldspar ages obtained for a given sample, because it could help us to qualitatively assess the past level of bleaching of the grains, since the measured signals have different bleaching rates (Godfrey-Smith et al., 1988; Murray et al., 2012). The quartz OSL signal is known to bleach more rapidly than the IR_{50} signal from feldspar, which itself bleached faster than the pIR-IR_{225} signal. So, if the bleaching had been sufficient at deposition, we would expect that OSL, IR_{50} and pIR-IR_{225} signals provide similar ages; conversely, if the bleaching was insufficient, the obtained ages are expected to be ranked in this order: OSL < IR_{50} < pIR-IR_{225}. For our La Quina samples, the OSL, IR_{50} and pIR-IR_{225} ages are in good agreement for the majority of samples (considering the associated errors) which suggests that deposition occurred slowly enough for the bleaching of the quartz and feldspar signals before burial. However, one can also note that the pIR-

530 IR_{225} ages are either indistinguishable from the IR_{50} ages or slightly higher, which suggests
531 that even if the exposure to daylight was sufficient in most cases to bleach both the IR_{50} and
532 pIR-IR_{225} signals, sometimes it was not. This observation supports our confidence in the IR_{50}
533 ages.

534 There is, however, a noticeable exception to this. As already mentioned, sample
535 BDX 15271 (Layer M) has an OSL age which is largely underestimated compared to the IR_{50}
536 age. Possible causes underlying the underestimation of the OSL age are difficult to assess
537 given that the mineralogy and the grain size distribution are broadly identical in Layers L, M
538 and N. Furthermore, we do not consider that this huge difference (~20 ka) is caused by an
539 insufficient bleaching of the feldspar grains, since the IR_{50} ages show a remarkable
540 consistency all along the sequence (except for Layers G1 and G2). It might be important to
541 note that we are comparing ages obtained from feldspar grains present in the fine silt
542 fraction (20 - 41 µm) with those obtained from quartz grains present in the coarse sand
543 fraction (160 - 250 µm). The discrepancy between the OSL and IR_{50} ages could result from
544 spatial heterogeneities of the beta dose rate, which differentially affected the two size
545 fractions. At this stage, only a sedimentary contextual analysis based on a microscopic study
546 of the sediment would allow a better estimation of the distribution of these minerals within
547 this layer and an evaluation of its influence on the doses received by the analysed fractions.
548 Because the OSL age obtained for this layer is largely underestimated compared to the
549 overlying Layers, we consider that the event sought to date is accessible only with the
550 feldspar grains from this layer.

551 HERE Fig. 8

552

553

554 **5. Interpretation of the ages and regional implications**

555

556 Following the discussion above, a new chronological framework can be proposed for
557 the La Quina sequence. The IR_{50} ages on feldspar grains and the accepted OSL ages on quartz
558 can be compared with the radiocarbon and TL ages previously obtained (Fig 9). All these
559 ages are broadly coherent and follow the stratigraphy.

560 The base southern section yields a succession of human occupations at the end of
561 MIS 4 and the beginning of MIS 3 around 63 – 55 ka (Fig 9). This time range is consistent with
562 the presence of reindeer within the southern section, indicating open, dry arctic conditions.
563 Turning to the northern section, the various results available from archaeology and
564 chronology (radiocarbon, TL, OSL and IRSL) lead to a much more detailed chronological

framework than has hitherto been possible. Based on these different datasets, we propose a chronological scenario of the last MP occupations of La Quina based on a Bayesian model incorporating both the radiocarbon dates previously published and the new ages presented here (see SOM). The results show a very strong level of agreement between the AMS radiocarbon determinations and the OSL and burnt flint TL ages. The only outlier in the model is a radiocarbon date (OxA-21806; Level 6a), which appears marginally younger in the model than it ought to be, probably due to modern carbon contamination. At the base of the northern section, Layer 8 starts at 50.3 – 48.2 ka (1σ probability range) and ends at 49.6 – 47.9 ka (1σ), it is a cold climatic period with abundant reindeer. The rockfall of Layer 7 may have occurred between 49.6 to 47.9 ka, and could be associated with the Heinrich 5 event (50 – 48 ka). Above, Layers 6d and 6c date to 47.5 – 45.0 ka (1σ) and give indications of a rapid climatic change toward open, non-arctic conditions, indicated by the presence of horses, large bovids and reindeer in less proportion. During later occupations, the climate changed from a steppe environment in Layer 5, towards an open temperate environment in Layers 4 and 2, indicated by the abundance of horse remains. This shift is dated to 43.2 – 42.0 ka (1σ). Finally, there is no evidence of human occupation after 40 ka at the site.

HERE Fig. 9

These dates from La Quina are important because they enable us to compare the chronometric sequence from here with other late Middle Palaeolithic sites that have played a part in the debate on the diversity of the Mousterian complex in Western Europe. One of the main features of this region is the multiplicity of technological behaviours reflected within the archaeo-stratigraphic sequences. Based on the systematic study of several major Mousterian assemblages, the diversity of the lithic industries led to five main facies being identified, based essentially on typology (e.g. Quina Mousterian, Ferrassie Mousterian, Mousterian of Acheulean Tradition, Typical Mousterian…). These were interpreted as reflecting cultural groups with different traditions who might have coexisted (Peyrony, 1930 ; Bordes, 1953, 1961 ; 1973). Other hypotheses have been proposed to explain this diversity (Mellars, 1965; Binford and Binford, 1966; Rolland and Dibble, 1990; Dibble and Rolland, 1992), but none of these has met with general acceptance. It seems reasonable to think that the diversity of Mousterian industries is linked to the variability of technological systems adopted by prehistoric groups. This may have differed through time according to skills and traditions, but may also have been a response to varied subsistence strategies and related mobility patterns (Delagnes, 2010; Delagnes & Rendu, 2011). In the 1930s, on the basis of the evidence from the so-called “classic” archaeo-sequences (Combe Grenal, Pech de l’Azé

599 and Moustier), Mellars (1965, 1969, 1970, 1988, 1996) proposed a regional archaeological
600 sequence of three Mousterian facies. According to this model the Quina industry is always
601 linked with reindeer dominated assemblages and hence appears restricted to a pleniglacial
602 climate, probably during MIS 4. Since then, many lithic assemblages have been studied
603 within this framework, expanding our knowledge of the variability inherent in each. These
604 critical reviews have led steadily to the replacement, at least in Europe, of the facies concept
605 with the so-called technocomplex lithic (TCL) concept, combining various aspects of: i) the
606 lithic production system, ii) the chaine opératoire, and iii) the technical objectives (Delagnes
607 and Meignen, 2006) with regard to the acquisition strategies and exploitation of lithic raw
608 material. Around 35 TCL concepts have been defined in western France (Jaubert, 2012).
609 Based on the hypothesis of the succession of technocomplexes in chronological order in the
610 sequences of the Charente and Perigord area, some recurrent successions of industry have
611 emerged when various sequences have been compared. A regional archaeological sequence
612 has been proposed (Jaubert et al., 2010, 2012; Discamps et al., 2011), supported by
613 climatostratigraphic and chronometric data. Following this model it appears that: i) the
614 Levallois technology is always associated with temperate fauna and dates from the MIS 5a,
615 ii) the Quina technology (or TCL) is reindeer dominant and dates from the end of the MIS 4,
616 and iii) the TCL with denticulates dates to MIS 3 where the fauna is temperate. These
617 attributions do not contradict the previous stratigraphic model established by Mellars (1969;
618 1996). However, these models suffer from the non-systematic revision of the lithic
619 assemblages and the criteria for their definition or differentiation have been established on
620 the basis of typological criteria which reflect only part of the lithic diversity (Faivre et al.,
621 2014). Consequently, the model produces discordant and sometimes contradictory results at
622 the local scale.

623 HERE Fig. 10

624 In order to identify any temporal patterning in the archaeological record, we report
625 in Fig. 10 the dates of the Quina production system available for well-dated sites of
626 southwestern France. The oldest evidence for the Quina production system in the region has
627 been found in Layer W-US22 at Chez Pinaud (also named Jonzac). Based on TL ages on flints,
628 the occupations here date to ~73 ± 3 ka (Richter, 2013), or the end of MIS 5 and beginning of
629 MIS 4. This suggests that the site was occupied just before La Quina. At Les Pradelles (also
630 named Marillac), a TL-age of 58 ± 5 ka (1σ) has been obtained in Facies 2b, which also
631 contains a Quina industry (Maureille et al., 2010). These dates indicate that the Quina

production system was being produced at the end of MIS 5 or the beginning of MIS 4, as well as during MIS 3 (before the H5 event -50-48 ka). For these three Charentian sequences, reindeer dominate, suggesting that dry and open arctic environments predominated. At Roc de Marsal (Dordogne), the Quina levels have been dated to between 61 ± 7 ka and 45 ± 4 ka (Layer 4; Guérin et al., 2012), or at the end of MIS 4 and in MIS 3. Similar results have been obtained in the same region for the Combe-Capelle Bas showing that the fires in which the flints were burnt belong to the early part of MIS 3 (Valladas, et al., 2003). It is interesting to note that during this period, other industries seem to be also present in the Dordogne region. In particular, the Ferrassie LTC (a scraper-rich industry with Levallois technology) has been recently dated from the end of MIS 4 and MIS 3 (Guérin et al., 2015) in the eponym site of La Ferrassie. Currently, the youngest Quina occurrences have been dated at Sous-les-Vignes at around ~45 ka. This site differs from the others due to its location (~ 120 km to the south, in the Lot et Garonne region) and the exclusive exploitation of bison. Hence, it seems that the Quina system persisted in southwestern France from MIS 5 to the first half of MIS 3, around 40 ka, with a chronological trend between areas: the Quina occupations in the Charente region seem older compare to those located in the Périgord.

At La Quina, the relative position of the Discoid production system layer is comparable with other sites where this system has been recognized. In the same sequence, the Discoid production systematically overlies the Quina, as at Placard, Combe-Grenal, Chadourne, Puycelsi, and Roc-en-Pail (Mellars, 1969, 1996). Two other sites that contain sequences where the Discoid system overlies the MTA with a Levallois production system are Saint-Césaire and Brouillaud. Even if both these systems seem to be systematically recognized in the top of the sequence in southwestern France, they have been insufficiently directly dated.

The patterns we summarize here suggest that Levallois, Quina and Discoïd lithic production systems are part of late Middle Palaeolithic variability. This echoes the conclusions of Delagnes and Meignen (2006), in the sense that they suggest the possible presence of different human groups, with their own traditions and behaviour, in the same territory with a greater diversity from MIS 5 to MIS 3. Developments in numerical dating techniques and their application in MP and UP sites are all the more important to help us to address the interaction between human groups at the time of the Neanderthal extinction and the arrival of the modern human.

6. Conclusion

Our chronometric work at the La Quina site suggests that there was a continuous succession of human occupation throughout the entire sequence. The OSL, IRSL, TL and radiocarbon dates provide a robust and detailed chronology and show that the levels occupied by reindeer hunters and the makers of the Quina technocomplex date from the end of MIS 4 to the beginning of MIS 3. In contrast, levels containing a mainly Levallois industry date to MIS 4-3 in the southern section and MIS 3 in the northern section. The thin Layer 6d with a discoid production system dates to MIS 3. Finally, there is no evidence of human presence after 40 ka at the site. The results imply that the Quina production system was not restricted to MIS 4, as many have thought previously in light of the work of scholars such as Francois Bordes. The Quina probably begins during MIS 5 and intensifies during the first half of MIS 3 in several deposits in the southwest of France, with possible regional variation in Charente and Périgord. This study highlights the dangers of assuming that the same lithic techno-complexes are contemporary in this region during the Middle Palaeolithic. There may be other factors influencing the presence of these different lithic industries other than time. More work needs to be undertaken. Besides the obvious need to increase the number of dates of Middle Palaeolithic occupations, a critical review of important archaeological sequences may help us to better understand adaptation strategies and cultural change in European populations during this period.

Acknowledgments: The authors are grateful to the Aquitaine Region Council for funding this research, through the program entitled “La radioluminescence des feldspaths: un nouvel outil de datation des gisements archéologiques et des séquence quaternaires d’Aquitaine”. This work was also supported by the French National research Agency via the LaScArBx Labex (project number ANR-10-LABX-52). Frouin and Higham are supported by the European Research Council under the European Union’s Seventh Framework Programme (FP7/2007-2013) / ERC grant agreement n° [324139] “PalaeoChron”. In particular, we thank André Debénath who passed away on the 3rd of June 2016 when the paper was under review.

Table captions:

Table 1: Summary of available data on geology (after Jelinek, 2012), lithic industry and faunal analysis (after Armand, 1999) presented with relevant thermoluminescence (Mercier

and Valladas, 1998) and radiocarbon ages (Higham et al., 2014) from previous studies. The list of sediment samples collected for the present luminescence dating study also appears.

Table 2: Environmental dose rate data for the La Quina luminescence dating samples.

Table 3: Summary of the luminescence measurements and final ages of La Quina samples.

Figure captions:

Figure 1: Location of La Quina and Late Middle Palaeolithic sites mentioned in the text.

Figure 2: Schematic diagram of the section C of Station Amont at la Quina (after Jelinek, 2013. Schematic profil at locus 1 [Profile C]).

Figure 3: Plan of the site and location of the three loci (after Debénath and Jelinek, 1998)

Figure 4: General stratigraphic section of La Quina Amont, a) northern and b) southern deposits. Unit numbers are indicated on the drawings. OSL samples are indicated in blue and associated Al2O3:C dosimeters by orange circles.

Figure 5: Granulometric curves of the sediment samples used for luminescence dating.

Figure 6: Typical dose response curve measured on the sample BDX 15261, from a) the IR_{50} and b) the pIR-IR_{225} signals of the polymineral fraction and from c) the OSL signal of quartz. All dose response curves are fitted with a single exponential function. Distribution of the D_e determined for sample BDX 15261 using d) IR_{50}, e) pIR-IR_{225} and f) OSL signals.

Figure 7: OSL equivalent doses as a function of preheat temperature held for 10 s. For samples BDX 15263, the cutheat is fixed at 180 °C for and 160 °C for BDX 15267. Each point is an average of three previously bleached aliquots (3 hours under a solar simulator). The dashed line indicates the measured/given dose ratio. In both cases, the equivalent doses reach a plateau, indicating an independency with preheats.

Figure 8: Luminescence age results plotted in relationship with archaeological layer. IR_{50}

732 fading corrected ages (squares), pIR-IR_{225} ages (empty squares) of feldspar and OSL of quartz
733 (circles) are provided.
734
735 **Figure 9:** Summary of the luminescence ages of La Quina. IR_{50} fading corrected ages
736 (squares) of feldspar, OSL of quartz (circles), TL on flints (triangles) and calibrated
737 radiocarbon ages (solid line) are provided with 68.2% probability range. We consider the age
738 of sample BDX 15267 (Layer G2) and the OSL date of sample BDX 15271 (Layer M) as merely
739 indicative, in comparison to the other results and they appear in light grey. The grey solid
740 line represents the minimum estimation obtained with radiocarbon in Layer 8 (calibrated
741 result close to the age range limit). Thermoluminescence results are from Mercier and
742 Valladas (1999) and radiocarbon results are from Higham et al. (2014).
743
744 **Figure 10:** Summary of the dates available for the TCL Quina in southwestern France. A)
745 Localisation of the sites. B) In the Charente-Maritime region, only one site containing the TCL
746 Quina has been dated at the present time: the site of Chez-Pinaud (also named Jonzac). The
747 date of Layer US022 has been obtained by thermoluminescence on burnt flints (Richter et
748 al., 2013). In the Charente region, at La Quina, the date of each layer represents the sum of
749 probabilities of all the dates obtained in the present study, using IRSL (feldspar) and OSL
750 (quartz). At Les Pradelles (also named Marillac), only one TL date has been published so far
751 (Maureille et al., 2008). In the Dordogne region, different attempts to date the Roc de
752 Marsal site have been published. We report here the TL dates on burnt flints which are
753 believed to be more reliable than OSL results (see the discussion in Guérin et al., 2012). In
754 Combe-Capelle Bas, the TL dates are from Valladas et al. (2003). In Sous-les-Vignes, the
755 Quina occupations have been dated by ESR on teeth (Valladas et al., 1999).
756
757
758
759
760
761
762
763
764
765

References

Aitken, M.J., 1985. Thermoluminescence Dating. Academic Press, Orlando, Florida.

Auclair, M., Lamothe, M., Huot, S., 2003. Measurement of anomalous fading for feldspar IRSL using SAR. Radiation Measurements. 37, 487–492. https://doi.org/10.1016/S1350-4487(03)00018-0

Bierwirth, S.L., 1996. Lithic analysis in southwestern France: Middle Paleolithic assemblages from the site of La Quina. BAR international series. 633, IV, p. 75.

Binford, I., Binford, S., 1966. A preliminary analysis of functional variability in the Mousterian of Levallois faces, Americain Anthropologist. 68, 238‑295.

Bøtter-Jensen, L., McKeever, S.W.S., Wintle, A., 2003. Optically stimulated luminescence dosimetry. Elsevier, Amsterdam. pp. 374.

Bordes, F., 1953. Essai de classification des industries «moustériennes». Bulletin de la Société préhistorique française. 50, 547‑467.

Borde, F., 1973. On the chronology and contemporaneity of different Palaeolithic cultures in France, in The Explanation of Culture Change: Models in Prehistory, London: Duckworth, pp. 217‑260.

Bordes, F., 1961. Typologie du Paléolithique ancien et moyen, (Bordeaux, Imprimeries Delmas, pp. 85.

Bortolot, V.J., 2000. A new modular high capacity OSL reader system, Radiation Measurements. 32, 751‑757. https://doi.org/10.1016/S1350-4487(00)00038-X

Brennan, B.J., Lyons, R.G., Phillips, S.W., 1991. Attenuation of alpha particle track dose for spherical grains. Nucl. Tracks Radiat. Meas. 18, 249–253. https://doi.org/10.1016/1359-0189(91)90119-3

Buylaert, J.-P., Murray, A.S., Thomsen, K.J., Jain, M., 2009. Testing the potential of an elevated temperature IRSL signal from K-feldspar. Radiat. Meas. 44, 560–565. https://doi.org/10.1016/j.radmeas.2009.02.007

Buylaert, J.-P., Jain, M., Murray, A.S., Thomsen, K.J., Thiel, C., Sohbati, R., 2012. A robust feldspar luminescence dating method for Middle and Late Pleistocene sediments, Boreas. 41, 435‑451.

Chase, P.G., Armand, D., Debénath, A., Dibble, H., Jelinek, A.I., 1994. Taphonomy and zooarchaeology of a Mousterian faunal assemblage from La Quina, Charente, France. Journal of Field Archaeology. 21, 289-305.

Chen, R., Pagonis, V., Lawless, J.L., 2015. Time and dose-rate dependence of TL and OSL due to competition between excitation and fading, Radiation Measurements. 82, 115-121. https://doi.org/10.1016/j.radmeas.2015.09.006

Debénath, A., Jelinek A., 1998. Nouvelles fouilles à La Quina (Charente): Résultats préliminaires, Gallia Préhistoire. 40, pp. 29‑74.

Delagnes, A., Rendu, W., 2011. Shifts in Neandertal mobility, technology and subsistence strategies in western France. Journal of Archaeological Science. 38, 1771-1783. https://doi.org/10.1016/j.jas.2011.04.007

Delagnes, A., 2010. In: Conard, N., J., Delagnes, A., Settlement dynamics of the Middle Paleolithic and Middle Stone Age III, Kerns Verlag, Tubingen, pp. 611.

Delagnes, A., Meignen, L., 2006. Diversity of Lithic Production Systems During the Middle Paleolithic in France: Are There Any Chronlogical Trends?, in Transitions before the transition, New York, Springer, pp. 85‑107.

Dibble, H and Rolland, N., 1992. On assemblage variation in the Middle Paleolithic of western Europe: History, perspectives and a new synthesis. In: H. Dibble and P. Mellars, Editors. The Middle Paleolithic: Adaptationm Behavior, and Variability. Philadelphia: University of Pennsylvania Museum Monographs. 72, pp. 1-28.

Discamps, E., Jaubert, J., Bachellerie, F., 2011. Human choices and environmental constraints: deciphering the variability of large game procurement from Mousterian to Aurignacian times (MIS 5-3) in southwestern France, Quaternary Science Reviews. 30, 2755‑2775. https://doi.org/10.1016/j.quascirev.2011.06.009

Duller, G.A.T., 2007. Analyst.Manual.pp. 45

Faivre, J. Ph., Discamps, E., Gravina, B., Turq, A., Guadeli, J.-L., Lenoir, M., 2014. The conrtibution of lithic production systems to the interpretation of Mousterian industrial variability in south-western France: The example of Combe Grenal (Dordogne, France). Quaternary International. 350, 227-240. https://doi.org/10.1016/j.quaint.2014.05.048

Frouin, M., Lahaye, C., Hernandez, M., Mercier,N., Guibert, P., Brenet, M., Folgado-Lopez, M., Bertran, P., 2014. Chronology of the Middle Palaeolithic open-air site of Combe Brune 2 (Dordogne, France): a multiluminescence dating approach, Journal of Archaeological Science. 52, 524-534. https://doi.org/10.1016/j.jas.2014.09.012

Galbraith, R.F., Roberts, R.G., Laslett, G.M., Yoshida, H., Olley, J.M., 1999. Optical dating of single and multiple grains of quartz from Jinmium rock shelter, northern Australia: part I, experimental design and statistical models. Archaeometry. 41, 339-364.

Galbraith, R.F., Roberts, R.G. 2012. Statistical aspects of equivalent dose and error calculation and display in OSL dating: An overview and some recommendations. Quaternary Geochronology. 11, 1-27. https://doi.org/10.1016/j.quageo.2012.04.020

Godfrey-Smith, D.I., Huntley, D.J., Chen, W.H., 1988. Optical dating studies of quartz and feldspar sediment extracts. Quat. Sci. Rev. 7, 373–380. https://doi.org/10.1016/0277-3791(88)90032-7

Guérin, G., Mercier, N., 2011. Determining gamma dose-rates by field gamma spectroscopy in sedimentary media: results of Monte Carlo simulations. Radiation Measurements. 46, 190-195. https://doi.org/10.1016/j.radmeas.2010.10.003

Guérin, G., Discamps, E., Lahaye, C., Mercier, N., Guibert, P., Turq, A., Dibble, H. L., McPherron, S. P., Sabdgather, D., Goldberg, P., Jain, M., Tjomsen, K., Patou-Mathis, M., Castel, J.-C., Soulier, M. C., 2012a. Multi-method (TL and OSL), multi-material (quartz and flint) dating of the Mousterian site of Roc de Marsal (Dordogne, France): correlating Neanderthal occupations with the climatic variability of MIS 5-3, Journal of Archaeological Science. 39, 3071‑3084. https://doi.org/10.1016/j.jas.2012.04.047

Guerin, G., Mercier, N., Nathan, R., Adamiec, G., Lefrais, Y., 2012b. On the use of the infinite matrix assumption and associated concepts: A critical review. Radiat. Meas. 47, 778-785. https://doi.org/10.1016/j.radmeas.2012.04.004

Guérin, G., Frouin, M., Talamo, S., Aldeias, V., Chiotti, L., Dibble, H., Goldberg, P., Hublin, J.J., Jain, M., Lahaye, C., Madelaine, S., Maureille, B., McPherron, S., Mercier, N., Murray, A., Sandgathe, D., Steele, T.E., Thomsen, K., Turq, A., 2015. A Multi-method Luminescence Dating of the Paleolithic Sequence of La Ferrassie Based on New Excavations Adjacent to the La Ferrassie 1 and 2 Skeletons. Journal of Archaeological Science. 58, 147-166. https://doi.org/10.1016/j.jas.2015.01.019

Guérin, G., Mercier, N., Adamiec, G., 2011. Dose-rate conversion factors: update. Ancient TL. 29 (1), 5–8.

Guibert, P., Schvoerer, M., 1991. TL dating: low background gamma spectrometry as a tool for the determination of the annual dose. Nucl. Tracks Radiat. Meas. 18, 231–238. https://doi.org/10.1016/1359-0189(91)90117-Z

Guibert, P., Bechtel, F., Bourguignon, L., Brenet, M., Couchoud, I., Delagnes, A.,Delpech, F., Detrain, L., Duttine, M., Folgado, M., Jaubert, J., Lahaye, C., Lenoir, M., Maureille, B., Texier, J.-P., Turq, A.,Vieillevigne, E., Villeneuve, G., 2008. Une base de données pour la chronologie du Paléolithique moyen dans le Sud-Ouest de la France. Mémoire XLVII de le Société Préhistorique Française, 19-40.

Henri-Martin, G., 1966. Découverte d'un temporal humain néendertalien dans le Moustérien de la Quina, Charente, C. R. Acad. Sc. Paris, série D, 262, 1937‑1939.

Higham, T., 2011. European Middle and Upper Palaeolithic radiocarbon dates are often older than they look: problems with previous dates and some remedies, Antiquity. 85, 235-249. https://doi.org/10.1017/S0003598X00067570

Higham, T.F.G., Douka, K., Wood, R., Bronk Ramsey, C., Brock, F., Basell, L., Camps, M., Arrizabalaga, A., Baena, J., Barroso-Ruíz, C., Bergman, C., Boitard, C., Boscato, P., Caparrós, M., Conard, N.J., Draily, C., Froment, A., Galván, B., Gambassini, P., Garcia-Moreno, A., Grimaldi, S., Haesaerts, P., Holt, B., Irix-Chiapusso, M-J., Jelinek, A., Jordá Pardo, J.F., Maíllo-

Fernández, J-M., Marom, A., Maroto, J., Menéndez, M., Metz, L., Morin, E., Moroni, A., Negrino, F., Panagopoulou, E., Peresani, M., Pirson, S., de la Rasilla, M., Riel-Salvatore, J., Ronchitelli, A., Santamaria, D., Semal, P., Slimak, L., Soler, J., Soler, N., Villaluenga, A., Pinhasi, R., Jacobi., R., 2014. The timing and spatio-temporal patterning of Neanderthal disappearance. Nature. 512, 306–309.

Huntley, D.J., Baril, M.R., 1997. The K content of the K-feldspars being measured in optical dating or in thermoluminescence dating. Ancient TL. 15, 11–13.

Huntley, D.J., Hancock, R.G.V., 2001. The Rb contents of the K-feldspar grains being measured in optical dating. Ancient TL. 19, 43–46.

Huntley, D.J., Lamothe, M., 2001. Ubiquity of anomalous fading in K-feldspars and the measurement and correction for it in optical dating. Can. J. Earth Sci. 38, 1093–1106.

Huot, S., Lamothe, M., 2012. The implication of sodium-rich plagioclase minerals contaminating K-rich feldspars aliquots in luminescence dating. Quaternary Geochronology. 10, 334-339. https://doi.org/10.1016/j.quageo.2012.03.003

Jaubert, J., 2010. Les archéoséquences du Paléolithique en Poitou-Charentes, in Préhistoire entre Vienne et Charente, hommes et sociétés du paléolithique, Mémoire 38, Chauvigny, pp. 51‑55.

Jaubert, J., 2012. Les archéo-séquences du Paléolithique moyen du Sud-Ouest de la France : quel bilan un quart de siècle après François Bordes?, in F. Delpech et J. Jaubert (dir.) - François Bordes et la Préhistoire. Actes du colloque international François Bordes, Bordeaux, 22-24 avril 2009, coll. Documents Préhistoriques, Bordeaux, pp.235‑253.

Jelinek A.J., 2013. Neandertal lithic industries at La Quina, Tucson, University of Arizona Press, pp.456.

Kars, R.H., Walinga, J., Cohen, K.M. 2008. A new approach towards anomalous fading correction for feldspar IRSL dating - tests on samples in field saturation. Radiation Measurements. 43, 786-790. https://doi.org/10.1016/j.radmeas.2008.01.021

Lamothe, M., Auclair, M., Hamzaoui, C., Huot, S., 2003. Towards a prediction of long-term anomalous fading of feldspar IRSL. Radiat. Meas. 37, 493–498. https://doi.org/10.1016/S1350-4487(03)00016-7

Li, B., Li, S.H.2008. Investigations of the dose-dependent anomalous fading rate of feldspar from sediments. J. Phys. D-Appl. Phys. 41 (22), pp.225502. https://doi.org/10.1088/0022-3727/41/22/225502

Liritzis, I., Singhvi, A.K., Feathers, J.K., Wagner, G.A., Kadereit, A., Zacharias, N., Li, S.- H., 2013. Luminescence Dating in Archaeology, Anthropology, and Geo- archaeology: an overview. Springer, Heidelberg, pp.70

Maureille B., Mann A., Beauval C., Bordes J.-G., Bourguignon L., Costamagno S., Couchoud I., Fauquignon J., Garralda M. D., Geigl E.-M., Grün R., Guibert P., Lacrampe-Cuyaubère Fr., Laroulandie V., Marquet J.-Cl., Meignen L., Mussini C., Rendu W., Royer A., Seguin G. et Texier J.-P., 2010. Les Pradelles à Marillac-le-Franc (Charente). Fouilles 2001-2007 : nouveaux résultats et synthèse. In Buisson-Catil J. et Primault J. (éds), *Préhistoire entre*

Vienne et Charente. Hommes et sociétés du Paléolithique. Association des publications chauvinoises, mém. XXXVIII. Chauvigny : APC, pp. 145-162.

Martin, L., Mercier, N., Incerti, S., Lefrais, Y., Pecheyran, C., Guérin, G., Jarry, M., Bruxelles, L., Bon, F., Pallier, C., 2015. Dosimetric study of sediments at the beta dose rate scale: Characterization and modelization with DosiVox software, Radiation Measurements 81, 134-141. https://doi.org/10.1016/j.radmeas.2015.02.008

Martin H., 1923. Recherches sur l'évolution du Moustérien dans le gisement de la Quina (Charente). Industrie lithique. Schleicher frères (Paris), O. Doin (Angoulême), Impr. ouvrière.

Mellars, P., 1965. Sequence and Development of Mousterian Traditions in South-Western France. Nature 205, 626–627.

Mellars, P., 1969. The Chronology of Mousterian Industries in the Perigord Region. Proceedings of the Prehistoric Society 35, 134-171

Mellars, P., 1970. Saille comments on the notion of "functional variability" in stone-tool assemblages. World Archaeology 2, 74-89.

Mellars P., 1988. The origins and dispersal of modern humans, Current Anthropology, 29, pp. 186‑188. http://www.jstor.org/stable/2743333.

Mellars, P., 1996. The neanderthal legacy: An archaeological perspective from western Europe. Princeton, N. J. pp. 480.

Mercier, N., Valladas, H., 1998. Datations, Gallia Préhistoire, 40, pp. 70‑71.

Mercier, N., Valladas, H., Valladas, G., 1994. A new dosimetric calibration tool. Nuclear Tracks and Radiation Measurements 23, 507-508.

Mercier, N., Wengler, L., Valladas, H., Joron, J.L., Froget, L., Reyss, J.L., 2007. The Rhafas Cave (Morocco): Chronology of the mousterian and aterian archaeological occupations and their implications for Quaternary geochronology based on luminescence (TL/OSL) age determinations, Quaternary Geochronology 2, 309‑313. https://doi.org/10.1016/j.quageo.2006.03.010

Morthekai, P., jain, M., Gach., G., Elema, D.R., Prip, H., 2013. Dependence of (anomalous) fading of infra-red stimulated luminescence on trap occupancy in feldspars, Journal of Luminescence 143, 704-709.

Murray, A.S., Thomsen, K.J., Masuda, N., Buylaert, J.P., Jain, M., 2012. Identifying well-bleached quartz using the different bleaching rates of quartz and feldspar luminescence signals. Radiation Measurements 47, 688–695. https://doi.org/10.1016/j.radmeas.2012.05.006

Nathan, R.P., Mauz, B., 2008. On the dose-rate estimate of carbonate-rich sediments for trapped charge dating. Radiation Measurements 43, 14–25. https://doi.org/10.1016/j.radmeas.2007.12.012

Olley, J.M., Pietsch, T., Roberts, R.G., 2004. Optical dating of Holocene sediments from a variety of geomorphic settings using single grains of quartz. Geomorphology 60, 337-358. https://doi.org/10.1016/j.geomorph.2003.09.020

Park S.-J., 2007. Systèmes de production lithique et circulation des matériere premiéres au Paléolithique moyen récent et final: Une approche techno-économique à partir de l'étude des industries lithiques de La Quina (Charente)., Thèse de Docteur de l'Université Paris X. pp.

Peyrony, D., 1930. Le Moustier, ses gisements, son industrie, ses couches géologiques, Revue Anthropologique 40, pp. 3‑76 et 155‑176.

Readhead, M.L., 2002. Absorbed dose fraction for 87Rb β particles. Ancient TL 20, 25–28.

Rees-Jones, J., 1995. Optical dating of young sediments using fine-grain quartz. Ancient TL 13, 9–14.

Richter, D., Hublin, J.-J., Jaubert, J., McPherron, S. P., Soressi, M., Texier, J.-P., 2013. Thermoluminescence dates for the Middle Palaeolithic site of Chez-Pinaud Jonzac (France), Journal of Archaeological Science 40, 1176‑1185. https://doi.org/10.1016/j.jas.2012.09.003

Roberts, R.G., Galbraith, R.F., Yoshida, H., Laslett, G.M., Olley, J.M., 2000. Distinguishing dose populations in sediment mixtures: a test of single-grain optical dating procedures using mixtures of laboratory-dosed quartz. Radiation Measurements 32, 459-465. https://doi.org/10.1016/S1350-4487(00)00104-9

Rolland, N., Dibble, H., 1990. A new synthesis of middle paleolithic assemblage variability, American Antiquity, 55, 480‑99. http://www.jstor.org/stable/281279

Stefan, V.H., Trinkaus, E., 1998. La Quina 9 and Neandertal mandibular variability, Bull. et Mém. de la Société d'Anthropologie de Paris, t. 10, 3-4, pp. 293-324.

Spooner, N.A., 1994. The anomalous fading of infrared-stimulated luminescence from feldspars, Radiation Measurements, 23, p.p. 625‑632. https://doi.org/10.1016/1350-4487(94)90111-2

Thomsen, K.J., Murray, A.S., Bøtter-Jensen, L., Kinahan, J., 2007. Determination of burial dose in incompletely bleached fluvial samples using single grains of quartz. Radiation Measurements 42, 370-379. https://doi.org/10.1016/j.radmeas.2007.01.041

Tribolo, C., Mercier, N., Valladas, H., 2001. Alpha sensitivity determination in quartzite using an OSL single aliquot procedure, Ancient TL 19, 47‑50.

Tsukamoto, S., Denby, P.M., Murray, A.S. Botter-Jensen, L., 2006. Time-resolved luminescence from feldspars: new insight into fading. Radiation Measurements 41, 790-795. https://doi.org/10.1016/j.radmeas.2006.05.013

Valladas, H., Mercier, N., Falguères, C., Bahain, J.-J., 1999. Contribution des méthodes nucléaires à la chronologie des cultures paléolithiques entre 300 000 et 35 000 ans BP, Gallia préhistoire 41, 1, 153‑166.

Valladas, H., Mercier, N., Joron, J. L., McPherron, S. P., Dibble, H., Lenoir, M., 2003. TL dates for the Middle Paleolithic site of Combe-Capelle Bas, France, Journal of Archaeological Science 30, 1443‑1450. https://doi.org/10.1016/S0305-4403(03)00039-6

Verna, C. Hublin J.-J., Debénath A., Jelinek A.J., Vandermeersch B., 2010. Two new hominin cranial fragments from the Mousterian levels at La Quina (Charente, France), Journal of Human Evolution 58, 3, 273‑278.

Verna, C., 2007. Une sépulture à La Quina (Charente)? Retour aux données, in Evin, Jacques (Ed.), Un siècle de construction du discours scientifique en préhistoire: XXVIe Congrès Préhistorique de France - Congrès du Centenaire de la Société Préhistorique Française; Avignon, 21 - 25 septembre 2004; actes, Vol. 3., pp. 527-535.

Vieillevigne, E., Bourguignon, L., Ortega, I., Guibert, P., 2008. Analyse croisée des données chronologiques et des industries lithiques dans le grand sud-ouest de la France (OIS 10 . 3), Paleo, 145‑166.

Visocekas, R., 1979. La luminescence de la calcite après irradiation cathodique: thermoluminescence et luminescence par effet tunnel, Université de Pierre et Marie Curie, (France), pp. 259.

Visocekas, R., 1985. Tunnelling radiative recombination in labradorite: Its association with anomalous fading of thermoluminescence. Nucl. Tracks 10, 521–529.

Wintle, A.G., 1997. Luminescence dating: laboratory procedures and protocols. Radiation. Measurements. 27, 769–817. https://doi.org/10.1016/S1350-4487(97)00220-5

Zhou, H., Zhao, J.-X., Feng, Y., Chen, Q., Mi, X., Shen, C.-C., He, H., Yang, L., Liu, S., Chen, L., Huang, J., Zhu, L., 2014. Heinrich event 4 and Dansgaard/Oeschger events 5–10 recorded by high-resolution speleothem oxygen isotope data from central China, Quaternary Research 82 (2), 394-404. https://doi.org/10.1016/j.yqres.2014.07.006

Table 1

Summary of available data on geology (after Jelinek, 2012), lithic industry and faunal analysis (after Armand, 1999) presented with relevant luminescence and radiocarbon ages from previous studies. The list of sediment samples collected for the present luminescence dating study also appears.

Layer	Description	Lithic Industry	Faunal remains[a]	Previous chronological studies		New Luminescence samples
				Radiocarbon	Luminescence	
				Age (ka cal BP – 95.4%)	Age TL/OSL (ka)	BDX
Northern deposit						
1	Organic soil that covers the entire slope surface			-	-	-
2	Relatively loosely consolidated deposit of limestone éboulis clasts of varying size and frequency in a matrix of sandy clays of deep yellow ochre hue	Dominant or exclusive Levallois with denticulates Mousterian	335 *Equus caballus*, 118 Bovinae, 39 *Rangifer tarandus (n = 493)*	-	-	-
2a				-	-	-
2b				42.76-40.08 (OxA 2326-22)	-	
3	Composed of large horizontally bedded éboulis clasts with evidence of in situ frost cracking, little interstitial sediment				-	-
4	Primarily small éboulis clasts with occasional larger pieces and little interstitial sediment		553 *Equus caballus*, 285 Bovinae, 18 *Rangifer tarandus (n = 958)*	43.13-40.54 (OxA 22153)	-	-
5	Thin layer of somewhat eroded limestone plaquettes		*31 Rangifer tarandus*, 22 Bovinae, *4 Equus caballus (n = 58)*	47.70-42.67 (OxA 21805)	-	-
6	Dark gray to black mixture of natural sediment and heavily fragmented burned and undburned animal bone and flakes and chips of flint			-	-	-
6a			611 Bovinae, *243 Rangifer tarandus, 99 Equus caballus, 16 Cervis* sp. *(n = 971)*	42.65-39.93 (OxA 21806)	43.0 ± 3.6 (Q1– Q3)	15259
6b		Dominant Discoid production system		-	-	-
6c		Dominant or exclusive Levallois with denticulates Mousterian	225 Bovinae, *20 Equus caballus, 15 Rangifer tarandus,* 11 *Cervis* sp. *(n = 271)*	-	-	-
6d			70 Bovinae, *42 Rangifer tarandus, 21 Cervis* sp., *17 Equus caballus (n = 150)*	>45.15 (OxA 21808)	-	-
7	Yellowish layer of limestone éboulis		*536 Rangifer tarandus, 32 Equus caballus,* 27 Bovinae *(n = 595)*	65.43-43.86 (OxA 22155)	-	15261
8	Blackish layer similar to Layer 6		*2304 Rangifer tarandus, 169 Equus caballus,* 81 Bovinae *(n = 2558)*	>45.60 (OxA 21807)	44.5 ± 4.2 (Q14) 53.0 ± 5.0 (Q15)	15262
9	Surface of the colluvium underlying Layer 8.	n.d.		-	-	-
Southern deposit						
A	Uniform yellow-brown unstructured colluvium, underlying Layer 1, that contains scattered limestone pieces ranging in size from fine gravel to boulders	Dominant or exclusive Levallois with denticulates Mousterian		-	-	-
B	Discontinuous layer of moderate size limestone blocks			-	-	-
C	Gray-brown sediment with small limestone fragments and some larger plaquettes			-	-	15263
D	Brown layer			-	-	15265
D1						
D2						
E	Group of large limestone blocks in a matrix of pale brown porous sandy silts	n.d.		-	-	-

F	Red-brown layer	n.d.	High frequency of reindeer (~90%) Decreasing proportions of bison and horse to reindeed from Layer L (30%) to Layer F (10%)	-	-	-
G	Suite of three subbeds of fine slightly rounded éboulis well consolidated in a matrix of dark brown porous sandy silt, and pale gray layer.	Exclusive Quina production system *Quina Technocomplex*		-	-	
G1					-	15266
G2					-	15267
G3					-	-
H –I	*Outside of the area of excavation*			-	-	-
J	Pale brown sandy silt layer with small rounded éboulis			-	-	-
K	Larger limestome pieces			-	-	15269
L	Dark grayish brown layer of sandy clays and silts with lenses of limestone gravel			-	-	15270
M	Reddish to yellowish brown layer of silty clay			-	-	15271
N	Gray to greenish gray sandy clay with frequent moderately large éboulis clasts.			-	-	15272
O to R	Calcareous éboulis in fine pale yellow brown fluviatile sands with thin interstratified silts and clay lenses	*n.d.*		-	91.6 ± 10.1 101 ± 12	15273
Bedrock						

[a] Counts (NISP) of the major identified faunal remains from the northern deposit. Such analyses have not been done on the faunal remains found in the southern deposit.

Table 2

Environmental dose rate data for the La Quina luminescence dating samples.

Sample BDX	Layer	Sample Depth (m)	Water content (%)[a]	Radioelement content[b]				Dose rate (Gy/ka)						
				K (%)	U_{top} (eq. ppm)	U_{bottom} (eq. ppm)	Th (ppm)	Ext. gamma + cosmic[c]	Polymineral				Quartz	
									Ext. alpha	Ext. beta	Int. beta	Total	Ext. beta	Total
Northern deposit														
15259	6	1.10	15 ± 5	0.21 ± 0.01	1.59 ± 0.09	1.30 ± 0.03	3.07 ± 0.06	0.38 ± 0.05	0.14 ± 0.03	0.34 ± 0.01	0.11 ± 0.01	**0.97 ± 0.04**	0.31 ± 0.01	**0.68 ± 0.03**
15261	7	1.64	15 ± 5	0.24 ± 0.02	1.06 ± 0.10	0.88 ± 0.03	3.61 ± 0.07	0.44 ± 0.05	0.13 ± 0.03	0.32 ± 0.01	0.11 ± 0.01	**1.00 ± 0.05**	0.29 ± 0.01	**0.74 ± 0.03**
15262	8	2.00	15 ± 5	0.29 ± 0.02	1.42 ± 0.11	1.27 ± 0.03	3.71 ± 0.07	0.75 ± 0.05	0.15 ± 0.03	0.40 ± 0.01	0.11 ± 0.01	**1.41 ± 0.06**	0.36 ± 0.01	**0.83 ± 0.04**
Southern deposit														
15263	B	3.04	15 ± 5	0.25 ± 0.02	1.76 ± 0.12	1.32 ± 0.03	3.81 ± 0.07	0.43 ± 0.05	0.16 ± 0.03	0.38 ± 0.01	0.11 ± 0.01	**1.08 ± 0.05**	0.15 ± 0.01	**0.58 ± 0.03**
15265	D	3.96	15 ± 5	0.45 ± 0.02	2.07 ± 0.14	1.88 ± 0.04	6.32 ± 0.11	0.54 ± 0.05	0.24 ± 0.05	0.61 ± 0.01	0.11 ± 0.01	**1.51 ± 0.07**	0.56 ± 0.01	**1.10 ± 0.04**
15266	G1	4.13	15 ± 5	0.17 ± 0.02	0.88 ± 0.11	0.96 ± 0.03	3.09 ± 0.08	0.51 ± 0.05	0.12 ± 0.03	0.28 ± 0.01	0.11 ± 0.01	**1.02 ± 0.04**	0.25 ± 0.01	**0.76 ± 0.03**
15267	G2	4.45	15 ± 5	0.65 ± 0.02	2.07 ± 0.16	2.78 ± 0.05	9.71 ± 0.13	0.81 ± 0.09	0.37 ± 0.08	0.91 ± 0.02	0.11 ± 0.01	**2.20 ± 0.10**	0.83 ± 0.02	**1.64 ± 0.03**
15269	K	5.29	15 ± 5	0.39 ± 0.02	1.97 ± 0.13	1.72 ± 0.04	5.34 ± 0.09	0.52 ± 0.05	0.21 ± 0.05	0.54 ± 0.01	0.11 ± 0.01	**1.38 ± 0.06**	-	-
15270	L	5.71	15 ± 5	0.51 ± 0.02	2.80 ± 0.16	2.07 ± 0.04	7.71 ± 0.12	0.52 ± 0.04	0.28 ± 0.06	0.70 ± 0.02	0.11 ± 0.01	**1.62 ± 0.07**	0.64 ± 0.02	**1.16 ± 0.03**
15271	M	6.18	30 ± 5	0.36 ± 0.02	1.57 ± 0.13	1.68 ± 0.04	5.99 ± 0.10	0.71 ± 0.09	0.23 ± 0.05	0.53 ± 0.01	0.11 ± 0.01	**1.59 ± 0.05**	0.44 ± 0.01	**1.17 ± 0.02**
15272	N	6.30	30 ± 5	0.53 ± 0.02	2.70 ± 0.17	2.90 ± 0.04	12.0 ± 0.14	0.71 ± 0.09	0.38 ± 0.08	0.81 ± 0.02	0.11 ± 0.01	**2.01 ± 0.09**	-	-
15273	O - R	6.62	30 ± 5	0.76 ± 0.02	2.27 ± 0.16	2.63 ± 0.04	11.1 ± 0.14	1.05 ± 0.09	0.35 ± 0.08	0.90 ± 0.02	0.11 ± 0.01	**2.41 ± 0.08**	-	-

[a] Field water content, expressed as % of mass of water/dry mass of the sample.

[b] K, U and Th contents have been determined by high-resolution gamma spectrometry and low background.

[c] The gamma and cosmic dose rates were determined from the dose recorded by the dosimeters.

Table 3

Summary of the luminescence measurements and final ages of La Quina samples.

Sample BDX	Layer	Polymineral									Quartz		
		IR_{50}				$pIR\text{-}IR_{225}$					OSL		
		D_e ± se (Gy)	OD ± 1σ (%)	*g* value ± 1σ (%/decade)	Age ± 1σ (ka)	D_e ± se (Gy)	OD ± 1σ (%)	*g* value ± 1σ (%/decade)	Age ± 1σ (ka)	Age ± 1σ (ka)	D_e ± se (Gy)	OD ± 1σ (%)	Age ± 1σ (ka)
					fading corrected					*corrected for residual*			
Northern deposit													
15259	6	38.4 ± 1.1	0	2.68 ± 0.19	**51.4 ± 2.4**	47.4 ± 1.3	0	1.18 ± 0.32	54.6 ± 3.9 $_{fc}$	**51.6 ± 3.9 $_{fc}$**	30.6 ± 1.1	13 ± 2	**44.9 ± 2.5**
15261	7	41.0 ± 1.0	0	2.58 ± 0.42	**52.7 ± 4.5**	48.8 ± 1.1	4 ± 2	1.16 ± 0.28	54.4 ± 2.8 $_{fc}$	**51.5 ± 2.8 $_{fc}$**	36.9 ± 1.2	11 ± 2	**50.2 ± 2.8**
15262	8	60.6 ± 1.5	0	2.63 ± 0.15	**55.5 ± 2.2**	-	-	-	**-**	**-**	42.3 ± 1.8	15 ± 3	**51.0 ± 3.8**
Southern deposit													
15263	C	45.9 ± 1.2	3 ± 1	2.70 ± 0.26	**54.7 ± 2.6**	63.5 ± 1.0	2 ± 2	0.66 ± 1.72	58.7 ± 3.8	**56.3 ± 3.7**	34.6 ± 1.8	20 ± 3	**59.9 ± 4.4**
15265	D	64.3 ± 1.7	2 ± 2	1.79 ± 0.46	**51.6 ± 5.3**	93.0 ± 1.4	2 ± 2	n.m.	61.4 ± 4.0	**59.7 ± 4.0**	62.2 ± 1.8	8 ± 2	**56.5 ± 2.4**
15266	G1	51.8 ± 1.4	2 ± 3	2.16 ± 0.43	**62.8 ± 5.3**	77.4 ± 2.3	9 ± 3	1.03 ± 1.88	76.2 ± 4.8	**73.6 ± 4.6**	46.2 ± 2.0	18 ± 3	**61.0 ± 3.6**
15267	G2	79.4 ± 2.1	4 ± 1	2.68 ± 0.60	**46.7 ± 3.0**	120 ± 2.0	4 ± 1	0.76 ± 0.85	54.5 ± 3.9	**53.2 ± 3.8**	70.5 ± 4.1	20 ± 4	**43.1 ± 2.6**
15269	K	63.9 ± 1.7	2 ± 2	2.52 ± 0.48	**59.3 ± 5.2**	92.3 ± 2.4	5 ± 2	n.m.	66.7 ± 4.5	**64.8 ± 4.3**	-	-	**-**
15270	L	73.8 ± 1.6	0	2.60 ± 0.27	**58.2 ± 2.8**	109 ± 2.4	4 ± 2	0.79 ± 1.82	67.5 ± 4.7	**66.2 ± 4.7**	64.3 ± 3.5	20 ± 3	**55.6 ± 3.3**
15271	M	69.2 ± 1.9	5 ± 1	2.46 ± 0.60	**55.3 ± 3.8**	93.6 ± 1.8	3 ± 2	1.16 ± 0.21	65.6 ± 3.7 $_{fc}$	**63.8 ± 3.7 $_{fc}$**	45.8 ± 2.3	17 ± 3	**39.1 ± 2.8**
15272	N	88.4 ± 2.0	0	2.65 ± 0.58	**57.8 ± 2.8**	109 ± 2.9	5 ± 2	1.15 ± 0.25	60.5 ± 4.0 $_{fc}$	**59.1 ± 4.0 $_{fc}$**	-	-	**-**
15273	O - R	105 ± 2.2	0	2.54 ± 0.55	**55.5 ± 3.1**	-	-	-	-	**-**	-	-	**-**

The notation “n.m.” means that the fading rate has not been measured.

“fc” index means fading corrected ages.

The equivalent doses D_e have been measured with a preheat fixed at 240 °C for 10 s and a cutheat either at 180 °C (samples BDX 15259, 15262, 15263), or 160 °C (BDX 15267, 15270, 15271). For sample BDX 15261, the preheat was fixed at 260 °C for 10s and the cutheat at 180°C. For samples BDX 15265 and 15266, the preheat was at 280 °C and the cutheat at 160 °C.

The overdispersion (OD) has been calculated using the Central Age Model (Galbraith et al., 1999).

The residual dose is 3 Gy.

Figure1

Click here to download high resolution image

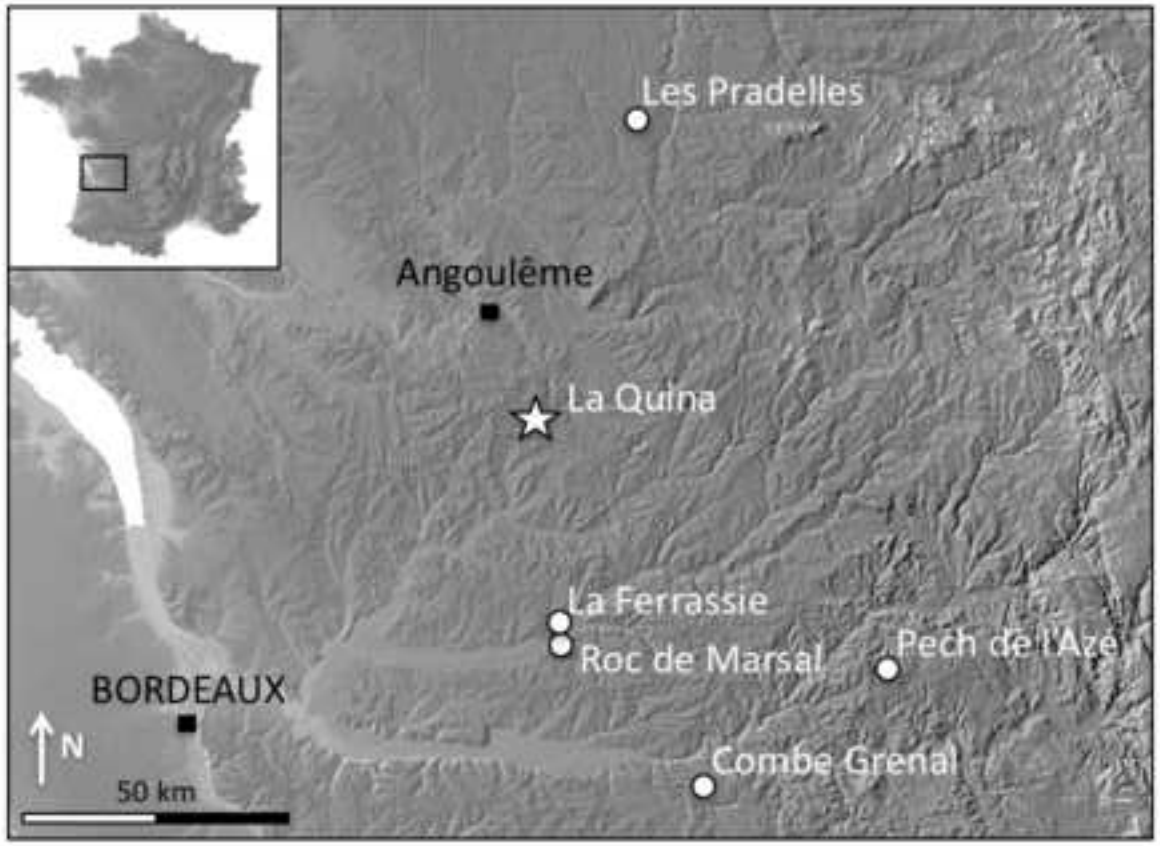


Figure2

Click here to download high resolution image

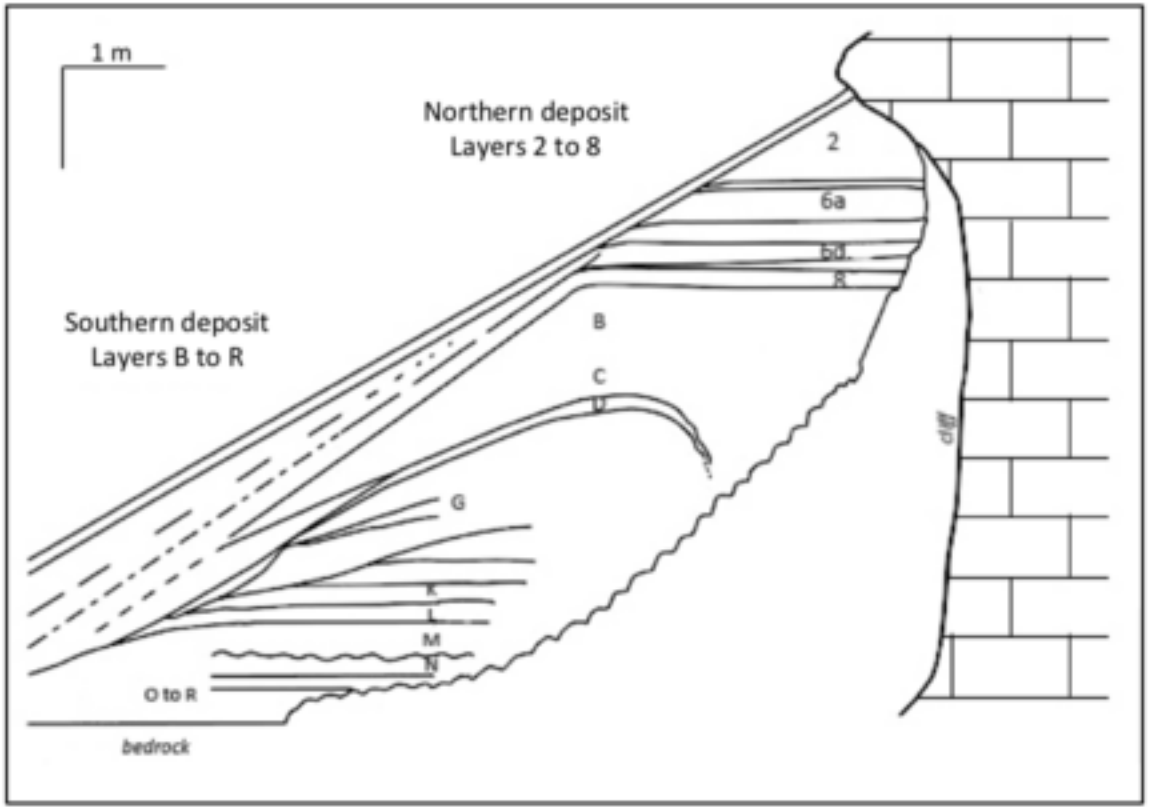


Figure3

Click here to download high resolution image

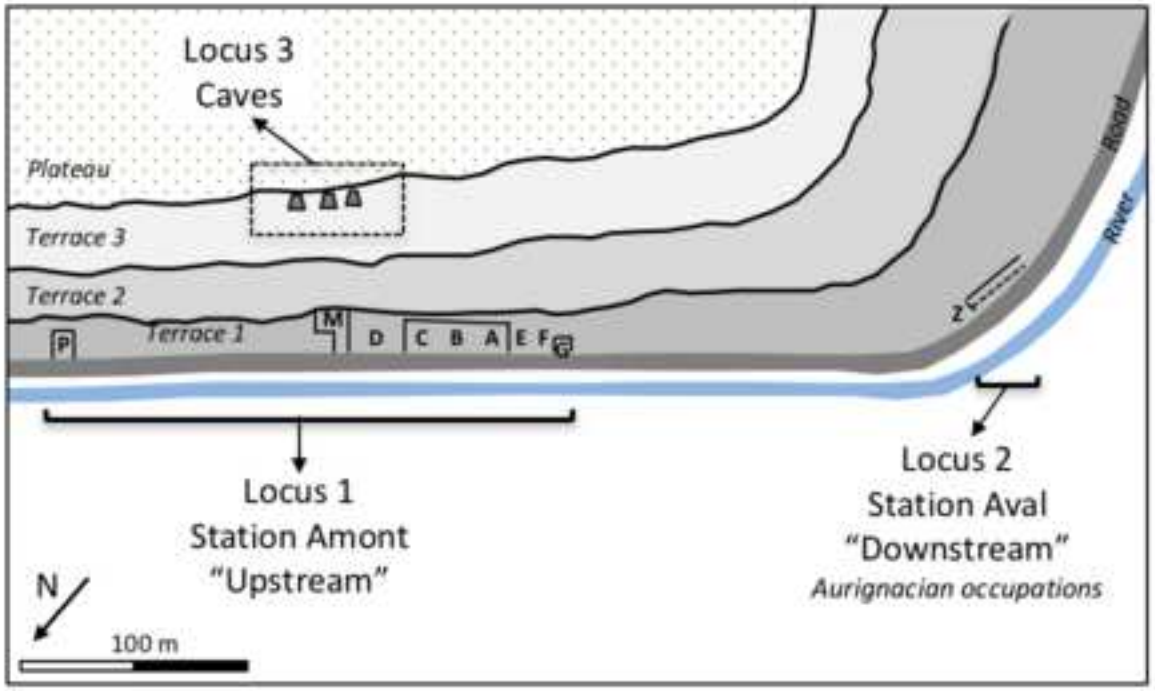


Figure4

Click here to download high resolution image

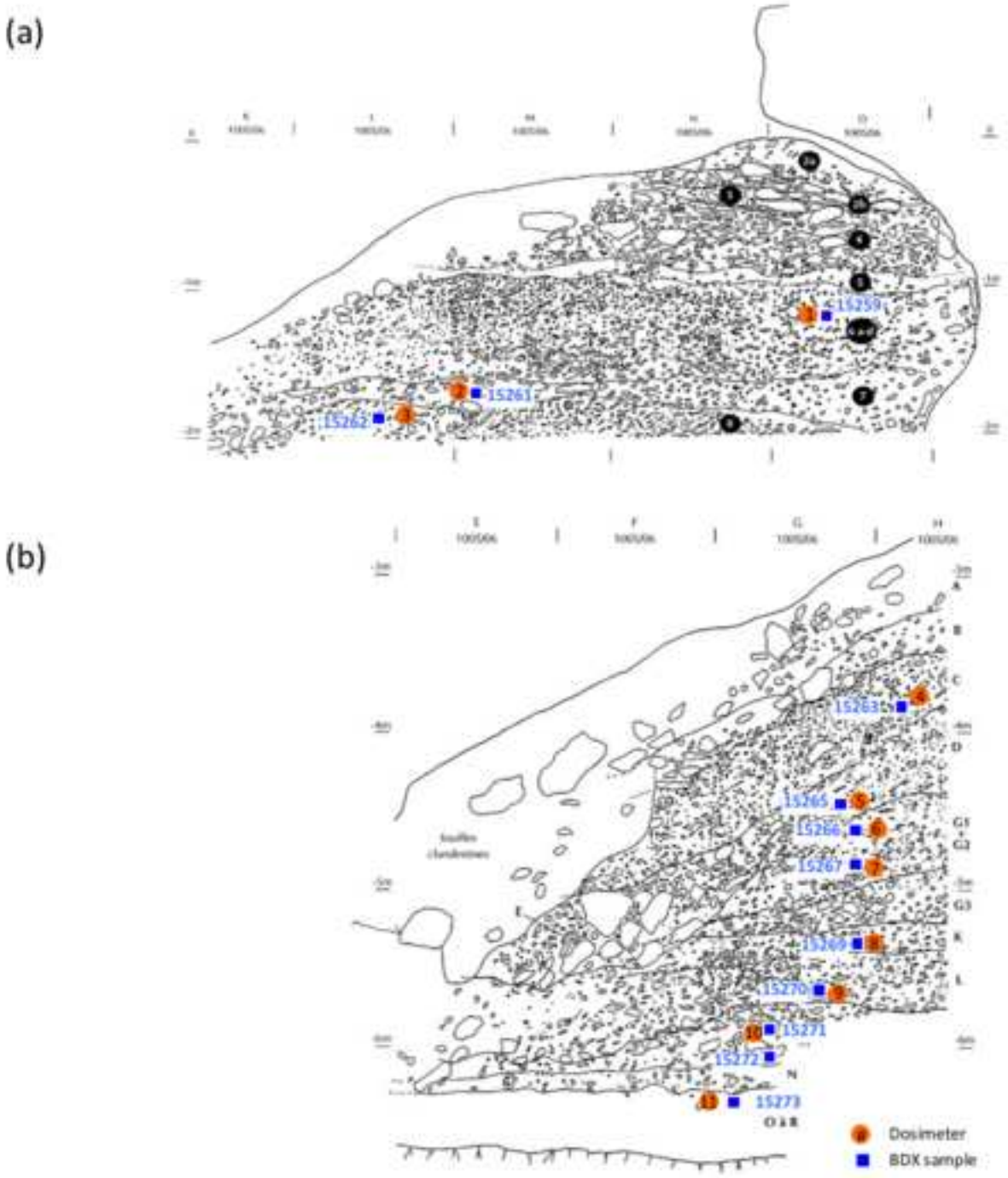


Figure5

Click here to download high resolution image

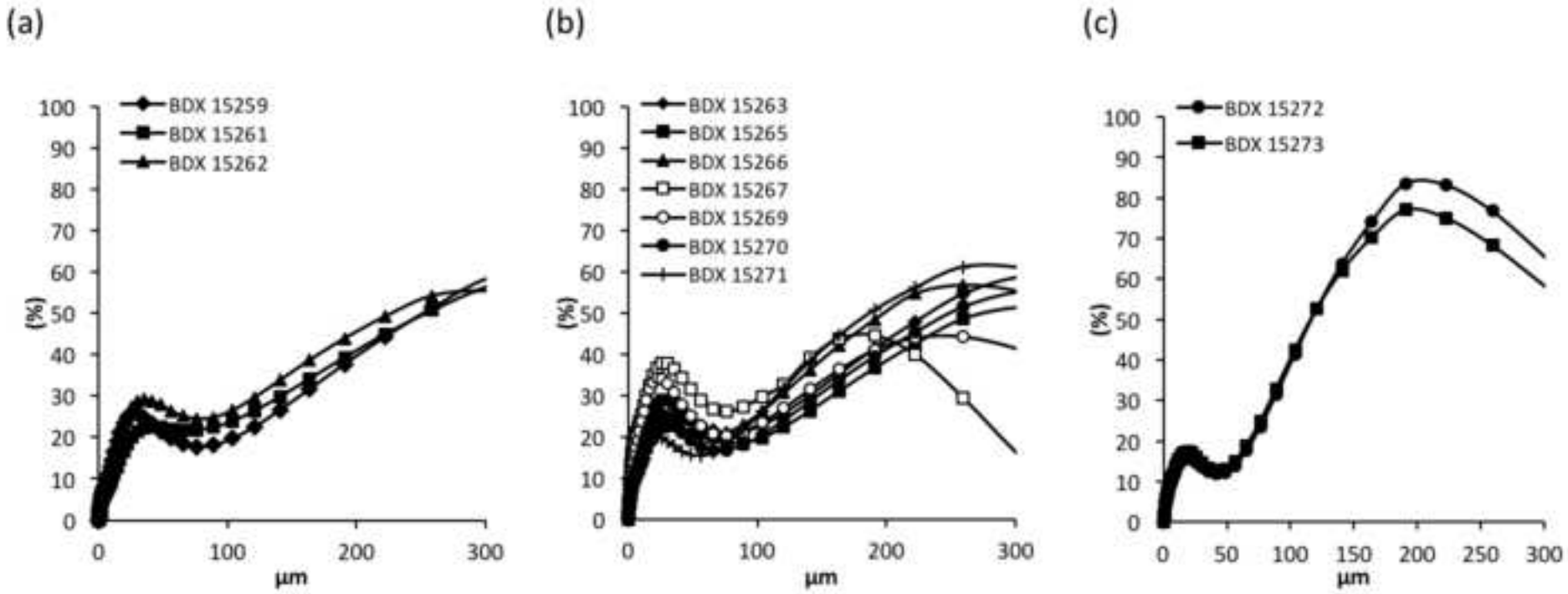


Figure6

Click here to download high resolution image

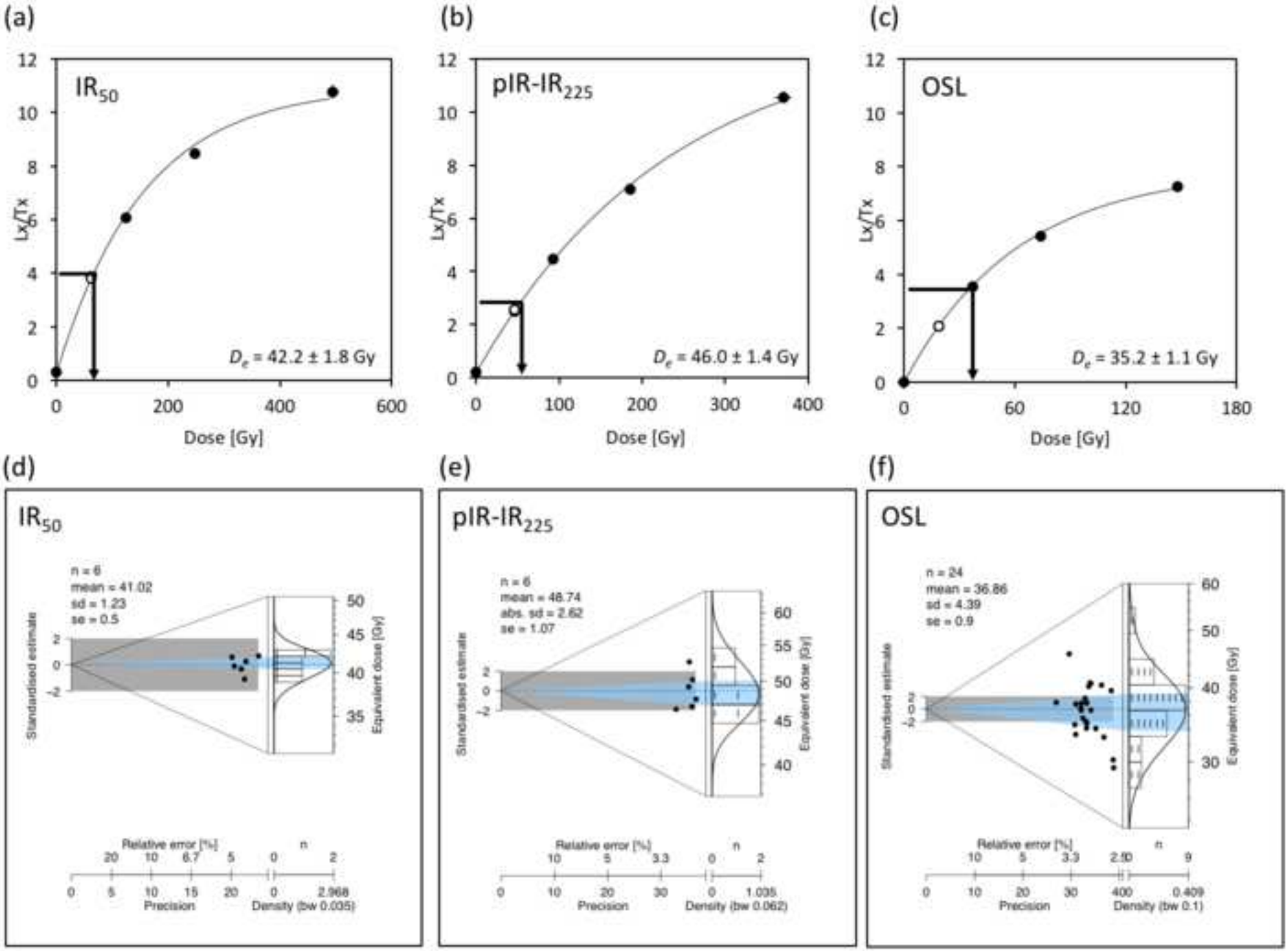


Figure7

Click here to download high resolution image

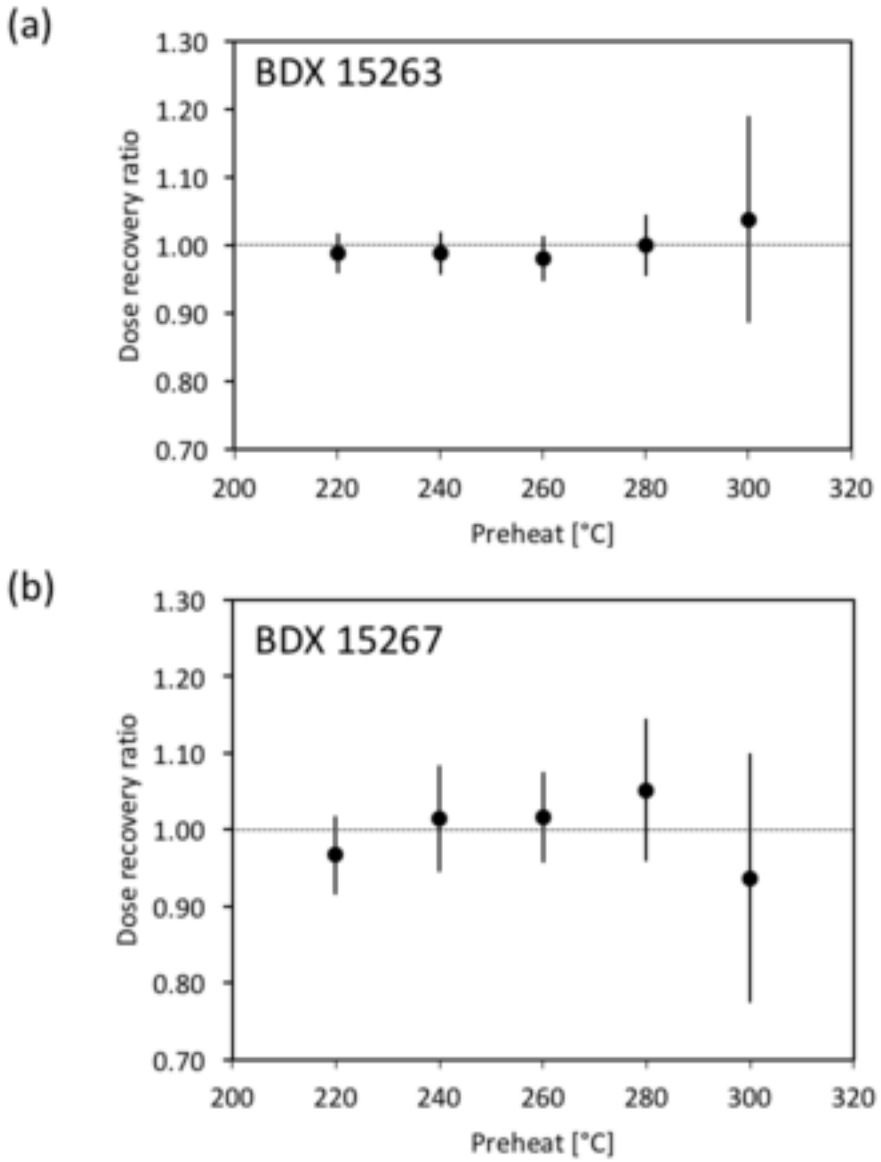


Figure8

Click here to download high resolution image

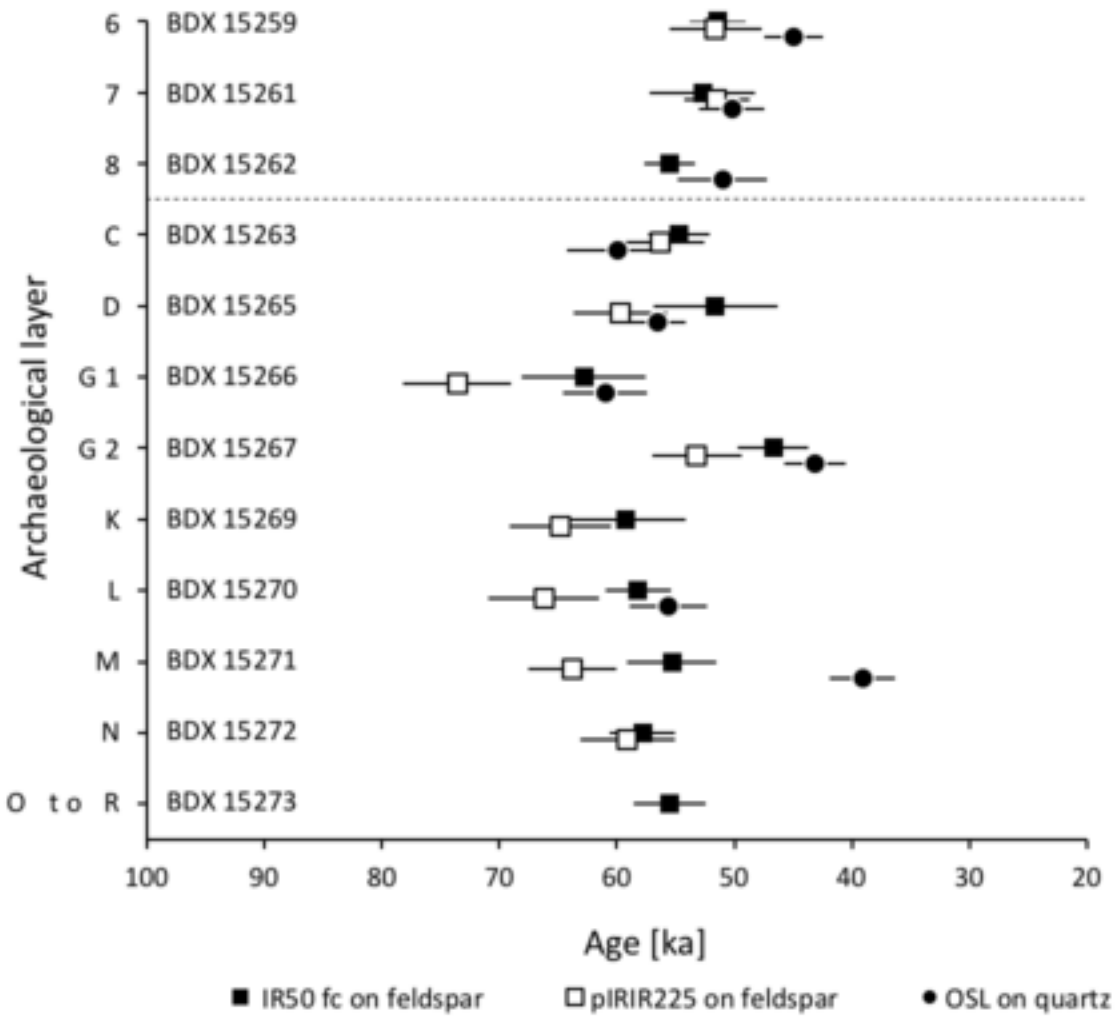


Figure9

Click here to download high resolution image

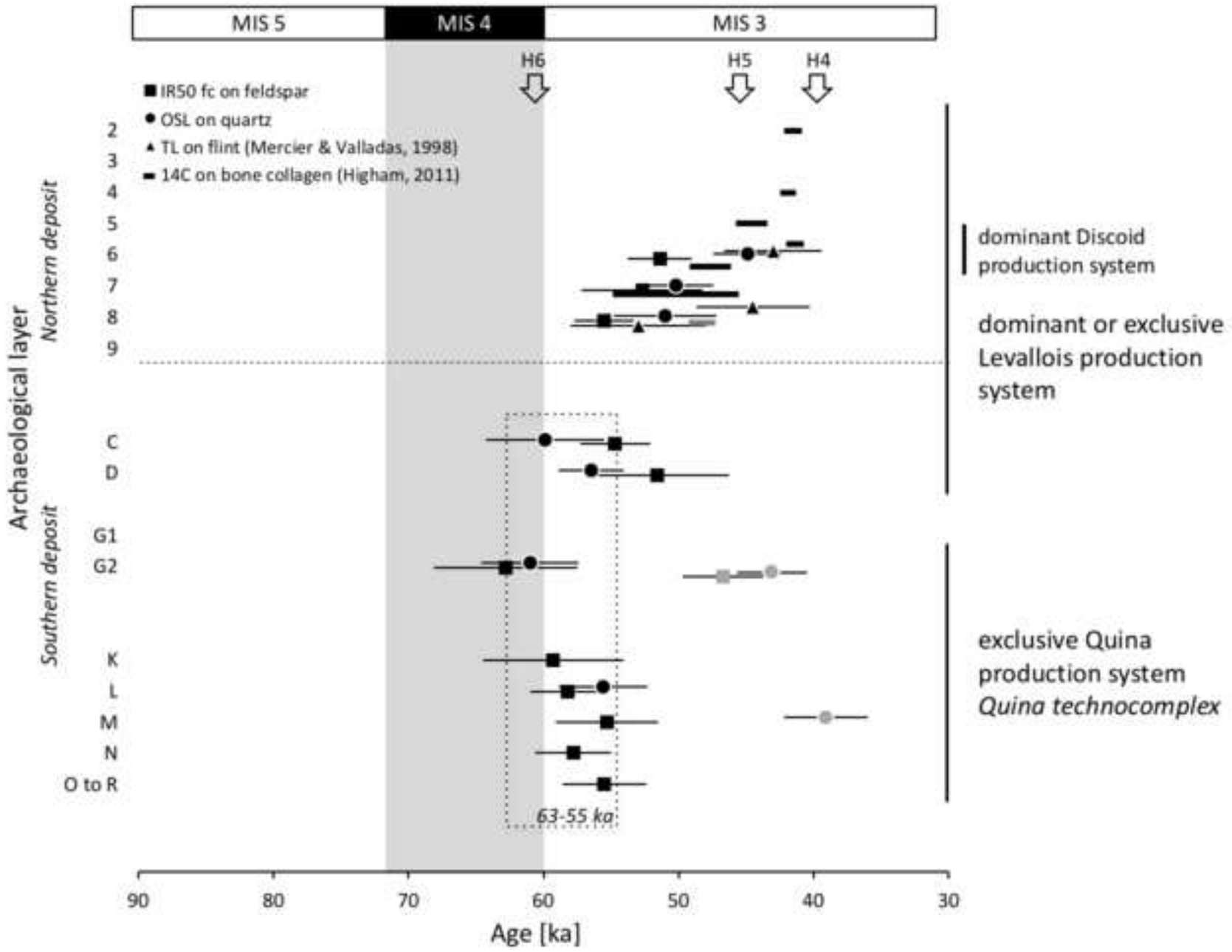
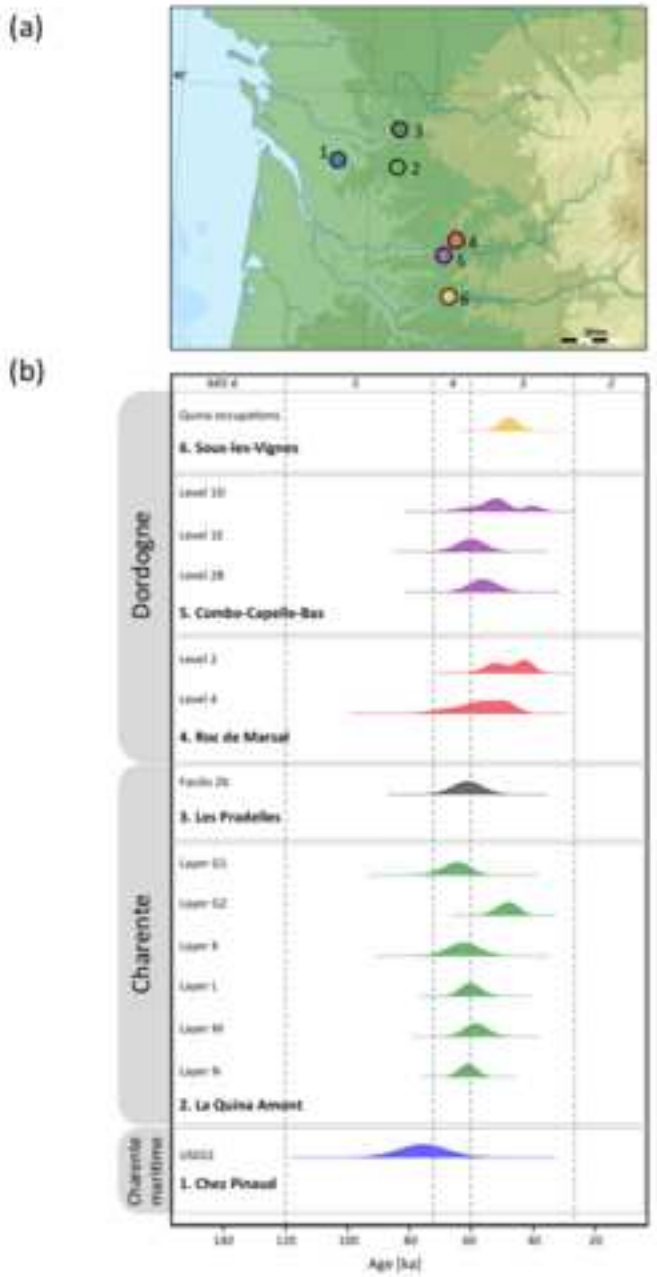


Figure10

Click here to download high resolution image



Supplementary Material

Click here to download Supplementary Material: SOM_AfterReview2_MF.doc